Cerebellar granular neuron progenitors exit their germinative niche via BarH-like1 activity mediated partly by inhibition of T-cell factor

Johnny Bou-Rouphael, Mohamed Doulazmi, Alexis Eschstruth, Asna Abdou, Beatrice Claude Durand

Cerebellar granular neuron progenitors exit their germinative niche via BarH-like1 activity mediated partly by inhibition of T-Cell Factor

Johnny Bou-Rouphael[1], Mohamed Doulazmi[2], Alexis Eschstruth[1], Asna Abdou[1] and Béatrice C. Durand[1, 2, 3, *]

[1] Sorbonne Université, CNRS UMR7622, Institut de Biologie Paris-Seine (IBPS) - Laboratoire de Biologie du Développement, 75005 Paris, France
[2] Sorbonne Université, CNRS UMR8256, Institut de Biologie Paris-Seine (IBPS) - Laboratoire Adaptation Biologique et Vieillissement, 75005 Paris, France
[3] Lead contact
* Correspondence: beatrice.durand@sorbonne-universite.fr (B.C.D)

SUMMARY

Cerebellar granule neuron progenitors (GNP) originate from the upper rhombic lip (URL), a germinative niche whose developmental defects produce human diseases. T-Cell Factors (TCF) responsiveness and Notch dependence are hallmarks of self-renewal in neural stem cells. TCF activity together with transcripts coding for proneural genes repressors *hairy and enhancer of split* (*hes/hey)*, are detected in the URL. However, their functions and regulatory modes are undeciphered. Here we established amphibian as a pertinent model to study vertebrate URL development. Amphibians long-lived URL is Tcf active, while the External Granular layer (EGL) is non-proliferative and expresses *hes4/5* genes. Using functional and transcriptomic approaches, we show that Tcf activity is necessary for URL emergence and maintenance. We establish that the transcription factor Barhl1 controls GNP exit from the URL acting partly through direct Tcf inhibition. Identification of Barhl1 target genes argues that besides Tcf, Barhl1 inhibits transcription of *hes5* genes independently of Notch signaling. Observations in amniotes suggest a conserved role of a *Barhl* in maintenance of the URL/EGL via coregulation of TCF and *hes/hey* genes.

KEYWORDS
Cerebellum; Rhombic Lip; Stem Cell; Tcf/Lef; Notch, Hes; BarH-like;

SUMMARY STATEMENT
We establish amphibian as a model to study Granular neuron (GN) development and that Barhl1 controls GN progenitor exit from their germinative niche through Tcf inhibition and *hes* genes repression.

INTRODUCTION

The Wnt/β-catenin cell-to-cell signaling pathway coordinates development and is one of the most conserved in the animal kingdom. The large majority of Wnt/β-catenin transcriptional targets are regulated by T-Cell Factor/Lymphoid Enhancer-binding Factor 1 (TCF/LEF1) transcription factors (TF) (reviewed in Bou-Rouphael and Durand, 2021; Hoppler and Waterman, 2014). Investigation of the developmental fate of Wnt/β-catenin-responsive cells in embryonic and postnatal mouse brains reveals that long-lived NSCs retain Wnt/β-catenin responsiveness throughout development (Bowman et al., 2013), and persistent TCF transcriptional activity appears to be a hallmark of long-lived NSC (reviewed in Ding et al., 2020; Nusse, 2008; Sokol, 2011; Urbán et al., 2019). Besides Wnt/TCF, the Notch pathway and its downstream effectors *hairy and enhancer of split* (*hes/hey)* that repress proneural genes expression, are required for maintenance of NSC, and a proper control of neurogenesis in both embryonic and adult brains (reviewed in Ables et al., 2011; Alunni and Bally-Cuif, 2016; Lampada and Taylor, 2023). Whereas TCF activation and Notch dependance appear to be hallmarks of both stem cell, and cancer stem cell, transcriptional cross regulations between the two pathways are poorly understood (Acar et al., 2021; Bayerl et al., 2021; Espinosa-Sánchez et al., 2020; Fendler et al., 2020).

A crucial component of the central nervous system (CNS) in all jawed vertebrates is the cerebellum, involved in executing motor functions as well as participating in higher cognitive processes such as decision-making, emotional and social behaviour, and expectation of reward (Reviewed in Reeber et al., 2013; Deverett et al., 2018; Carta et al., 2019; Haldipur et al., 2022). The cerebellum has two major stem cell niches: the ventricular zone (VZ) adjacent to the fourth ventricle, which produces all cerebellar GABAergic inhibitory neurons (Hoshino et al., 2005; Pascual et al., 2007; Yamada et al., 2014); and the upper rhombic lip (URL) which is the origin of glutamatergic excitatory neurons, derived from Atonal homologue 1 *(Atoh1)*-expressing progenitors. In amniotes, the URL gives birth first to the deep cerebellar nuclei (DCN), followed by the unipolar brush cells (UBC) and the granular neuron progenitors (GNP) that in turn produce granule neurons (GN), the predominant neuronal population in the entire CNS (Ben-Arie et al., 1997; Wang et al., 2005; Reviewed in Leto et al., 2016; Lackey et al., 2018; Joyner and Bayin, 2022). Defects in humans URL developmental program leads to serious diseases (Hendrikse et al., 2022; Smith et al., 2022; reviewed in Haldipur et al., 2022). Once they are born, GNPs undergo a tangential migration on the surface of the cerebellar plate, giving rise to the external granule layer (EGL).

Amphibians cerebellum displays morphological features resembling those found in higher vertebrates (Gona, 1972; Herrick, 1914) (reviewed in Hibi et al., 2017; Miyashita and Hoshino, 2022). Studies performed in the amphibian *Xenopus* at pre-metamorphosis stages reveal the presence of a non-proliferative EGL-like structure, which is unique compared with other anamniotes (Butts et al., 2014). These studies also indicate that the developmental processes that lead to the formation of GN, specifically the presence of an *Atoh1*-expressing URL and EGL, and the expression of the basic Helix Loop Helix (bHLH) neurogenic differentiation factor 1 (*Neurod1*), a marker of GN differentiation, are close to those described in higher vertebrates (Butts et al., 2014; D'Amico et al., 2013). Moreover, the amphibian URL maintains itself until post-metamorphic stages (Butts et al., 2014; Gona, 1972).

In the cerebellar primordium, while the VZ appears to be TCF inactive, positive TCF transcriptional activity has been documented in the URL of mice, human and *Xenopus* species (Borday et al., 2018; Garbe and Ring, 2012; Selvadurai and Mason, 2011; Wizeman et al., 2019). In the rodent EGL, Notch signalling maintains Sonic Hedgehog (SHH) dependent GNP

proliferation (Solecki et al., 2001; Machold et al., 2007; Adachi et al., 2021; reviewed in Miyashita and Hoshino, 2022). Whereas levels of Notch activity have been demonstrated to pattern the VZ in discrete subdomains (Khouri-Farah et al., 2022; Zhang et al., 2021), contributions of TCF and Notch to URL and early EGL biology and their regulatory modes have not been clearly identified.

ATOH1 directly induces its own expression as well as the expression of the two homeodomain (HD)-containing TF, *Barhl1* and *Barhl2*, which are mammalian homologues of the *Drosophila* Bar-class HD, BarH1 and BarH2 (reviewed in Bou-Rouphael and Durand, 2021; Reig et al., 2007). In the *Xenopus* organizer, Barhl2 binds to Tcf, and enhances Tcf repressor activity, thereby preventing β-catenin driven activation of Tcf target genes. Barhl2 maintains expression of Tcf target genes repressed by a mechanism that depends on histone deacetylase 1 (Juraver-Geslin et al., 2011; Sena et al., 2019a). In mice, *Barhl*1 and *Barhl2* transcripts are detected in the outer URL and the posterior EGL from E12.5 onwards (Aldinger et al., 2021; Bulfone, 2000; Kawauchi and Saito, 2008; Li et al., 2004; Mo et al., 2004). *Barhl1* participates in the generation of the EGL (Kawauchi and Saito, 2008), and is one of the major TF that regulate the radial migration of GNP in a mechanism involving Neurotrophin3 (NT3). Furthermore, an impairment in GN survival, and an attenuated cerebellar foliation, are observed in *Barhl1-/-* mice (Li et al., 2004). Although *Barhl2* is expressed in the amniote EGL (Mo et al., 2004), a potential role of *Barhl2* in cerebellar development has not been investigated, and whether BARHL1 interacts with, and regulates, TCF transcriptional activity is unknown.

Here, using *Xenopus* as a model system, we investigated the role of *Tcf* activity, and *barhl* genes in early GNP development. We establish that markers of GNP commitment and differentiation are conserved in *Xenopus* compared to amniotes and confirmed the presence of *atoh1* expressing EGL (Butts et al., 2014). We establish that the URL is proliferative, Tcf active and expresses *hairy and enhancer of split* (*hes*) 4 and 5. Whereas the EGL is non proliferative and displays low Tcf activity, it expresses high levels of *hes4* and *hes5*. Using gain and loss of function approaches (GOF/LOF), immunoprecipitation, and a *X. tropicalis* Wnt reporter transgenic line, we demonstrate that Tcf-mediated transcriptional activation is strictly necessary for URL emergence and maintenance. We did not detect *barhl2* in the *Xenopus* cerebellar anlage and focus our study on *barhl1*. We show physical interactions between Barhl1, Groucho(Gro)/Transducin-Like Enhancer of Split (TLE) and Tcf isoforms. Barhl1 overexpression phenocopies premature inhibition of Tcf, whereas Barhl1 LOF dramatically increases Tcf activity in the URL, leading to a major enlargement of the URL, and significant delays in GNP differentiation. Using a transcriptomic approach, we confirm that GNP depleted of Barhl1 stay in a proliferative, Tcf active, and *hes5* expressing state. We identify direct and indirect Barhl1 target genes in the cerebellar URL, and performed *in silico* analysis of Barhl1 target genes regulatory regions. Amongst the most upregulated target genes we identified markers of Tcf activity and of neural stemness, *hes/hey* genes, while down regulated genes are markers of neuronal differentiation. Our study establishes a Barhl TF as an inhibitor of Tcf activity and a repressor of some *hes/hey* genes that limits the size of a long lived germinative niche.

RESULTS

Spatial and temporal expression of key markers of GNP development are conserved in *Xenopus* compared to higher vertebrate

In amniotes the GNP developmental path is marked by expression of specific TF, including *Atoh1* which expression initiates in the RL, is maintained in the EGL during GNP proliferation, and is lost in differentiated GN that start expressing *Neurod1* (Flora et al., 2009; reviewed in Leto et al., 2016). In addition, the Paired box protein 6 (*Pax6*) and *Barhl1* expressions are markers of GNP commitment (Aldinger et al., 2021; Carter et al., 2018; Hanzel et al., 2019; Machold and Fishell, 2005; Miyata et al., 1999; Wizeman et al., 2019).

We performed ISH on *X. laevis* tadpoles through pre-metamorphic froglets, and assessed the expression of genes involved in the development of *Atoh1* lineage in rodents, focusing on GN. We used *pax6* (Fig. S1C), and *barhl1* (Fig. 1F) start of expression (stage 38) as a landmark of GNP induction. From stage 38 onwards, *atoh1* is expressed in the URL and in a layer of 3 to 4 cells bordering the URL which we considered part of the EGL (Fig. 1B; Fig. S.1A). *n-myc* is similarly expressed in the URL, but is also detected in the VZ (Fig. 1Ab, C, Fig. S1B). At both stage 42 and 48, *Hairy and enhancer of split (hes)-5 and hes4* (El Yakoubi et al., 2012; Grbavec et al., 1998), strongly labels part of the EGL (Fig. 1D). The dynamics of *pax6*, *barhl1*, and *neurod1* expressions within R1 from stage 38 to stage 48 reveals that they are first detected in the caudal region of the URL and EGL, and then in the cerebellar plate (Fig. 1E-G; Fig. S1C-E). At later stages their expression spread within the inner cerebellar tissue, where they undergo their final differentiation (Fig. 1E-G, Fig. S1D, E). While in amniotes *Orthodenticle Homeobox 2 (otx2)* expression is limited to the posterior lobes of the EGL, at stage 40 we detected *otx2* expression in the caudal EGL, which was subsequently extended to the cerebellar plate (Fig. 1H). In rhombomere 1 (R1) we detected *tcf7l1* transcripts mostly in the rostral URL, and part of the EGL, and to a lesser extent *tcf7* transcripts (Fig. S1G). We did not observe expression of *barhl2* in the cerebellar anlage at all developmental stages investigated (Fig. S1H).

These observations established a GNP development map that outlines the developmental progression of *atoh1* lineage cells within R1 (Fig. 1Ac). It reveals strong similarities between *Xenopus* and amniotes in the expression of genes involved in URL induction and specification/differentiation of GNP. As previously reported (Butts et al., 2014), we detect an EGL along the R1 antero-posterior axis which is marked by *atoh1*, *hes4* and *hes5.1*. Our observations also reveal a gradient in GNP differentiation, initiated in the caudal R1 at stage 38 and progressing to the rostral part up to stage 50.

Tcf inhibition, and Barhl1 overexpression, generate similar developmental defects in *atoh1* expression, URL induction and GNP early commitment/differentiation

We focused our study on the role of Tcf and Barhl1 in URL establishment and maintenance, during the time window when GNP are produced. Development of the URL and GNP was investigated using *atoh1*, and *pax6, barhl1*, *neurod1* as respectively URL/EGL, and GNP commitment /differentiation markers. We used *tcf7l1-Δβcat-GR*, an inducible form of *tcf7l1* which lacks its β-catenin binding domain, and thus acts as a inducible constitutive inhibitor of Tcf transcriptional activity (Molenaar et al., 1996) (Fig. S2).

At a high dose, *tcf7l1-Δβcat-GR* overexpression induced a dramatic reduction in the size of the URL, associated with the disappearance of the expression of its key marker *atoh1*. This effect is restricted to R1 (Fig. 2Aa-a", c). At a lower dose, *tcf7l1-Δβcat-GR* overexpression induced a decrease in *atoh1* expression (Fig. 2Ab, c). This decrease is associated with both an increase

of expression, and a rostral shift, observed with the three commitment/differentiation markers *pax6*, *barhl1*, and *neurod1* within R1 (Fig. 2Ba-d).
Similarly, *barhl1* overexpression phenocopies Tcf inhibition (Fig. S2). *barhl1* overexpression induced a decrease in *atoh1* transcripts levels within the URL (Fig. 2Ca-a", d), associated with an increase of *pax6* and *neurod1* expression, and a rostral shift in both markers' expression within R1 (Fig. 2Cb-d). Noteworthy, in both cases the loss of *atoh1* expression is limited to the R1 territory with no effect on isthmic nuclei or *atoh1* expression in R2 (Fig. 2Aa-a", c; 2Ca-a", c).
These data indicate that Tcf transcriptional activity is first necessary for the expression of *atoh1* within the URL, and second that once GNP are within the URL, premature inhibiting of Tcf activity leads to an accelerated GNP differentiation. Similarly, overexpression of *Barhl1* in the cerebellar primordium results in URL induction defects, associated with premature GNP differentiation.

In the cerebellar URL, inhibition of Barhl1 maintains GNP in an early progenitor state

To decrease Barhl1 activity within the cerebellar anlage, we designed and validated two morpholinos (MO), *MObarhl1-1* and *MObarhl1-2*, specifically targeting *Xenopus barhl1* mRNA (Fig. S2; S3; Methods). We investigated whether MO-mediated Barhl1 Knock-Down (KD) alters development of the URL, the EGL, and/or GNPs.
At all stage analyzed, depletion of Barhl1 induced an increase in *atoh1* expression, with *atoh1* expressing cells being expressed in the URL, and spreading across the surface of the cerebellar plate (Fig. 3Aa-a", Ba-a"; Fig. S3B, C, D). This expansion of *atoh1* expression territory is associated with an increase in *n-myc* expression (Fig. S3C), and a major decrease in both *pax6* and *neurod1* expression (Fig. 3Ab, Bb, C, Da-d; Fig. S3B, D). Furthermore, *barhl1* overexpression rescued the decrease in *neurod1* expression induced by Barhl1-KD (Fig. 3D).
We next asked whether inhibition of Tcf activity compensates for Barhl1-KD, using *pax6* as a marker of GNP commitment. As previously observed, Barhl1-KD delayed GNP differentiation process, while *tcf7l1-Δβcat-GR* overexpression accelerated it (Fig. 3Ea-c). Indeed *MObarhl1-1* co-injected with two different doses of *tcf7l1-Δβcat-GR* mRNA rescued the *pax6* expression defects (Fig. 3Ed-f).
These results indicate that Barhl1 depletion maintains GNP in an early progenitor state, and delays their differentiation. Barhl1-KD phenotype is rescued by inhibition of Tcf activity revealing that Barhl1 and Tcf act in opposing ways within the URL and the EGL.

Barhl1 limits Tcf transcriptional activity within the cerebellar primordium

We next asked whether Barhl1 directly controls Tcf transcriptional activity within the cerebellar URL. We investigated interactions between Barhl1, Groucho (Gro) 4, and Tcf isoforms, by performing co-immunoprecipitation experiments on protein extracts from HEK293T cells transfected with tagged constructs of Tcf7l1, Tcf7l2, Tcf7, Gro4, and Barhl1 (Fig. 4A). In agreement with Barhl1 containing two Engrailed Homology-1 (EH1) motifs known to interact with the WD-repeat domain of Gro, Barhl1 co-immunoprecipitated with Gro4 (Fig. 4Aa). Using Tcf7l1 as bait, we observed that Tcf7l1 immunoprecipitated Barhl1, in the presence and absence of Gro4 (Fig.4Ab). Finally, whereas Tcf7l1, Tcf7l2 and Tcf7 immunoprecipitated Barhl1, we observed that Tcf7l1 exhibited the highest efficiency in this process (Fig. 4Ac).
Concatemers of the consensus Tcf binding motif have been used to generate Wnt/Tcf reporter lines, such as *Xenopus tropicalis (X. tropicalis)* transgenic pbin7LefdGFP line (Borday et al., 2018; Tran and Vleminckx, 2014; Tran et al., 2010), which contains one copy of a *wnt* reporter gene. Using this reporter line, we assessed Tcf activity from stage 42 up to stage 50, and

observed a positive Tcf activity in the URL. Contrastingly, we did not detect any Tcf activity in the VZ and the EGL at similar developmental stages. Noteworthy, Tcf activity is stronger at the rostral end of the URL up to stage 48. This asymmetry of activity is lost at stage 50 (Fig. 4Ba-d). Similarly, *atoh1* is mostly detected in the rostral URL up to stage 50 where it starts to be expressed throughout the URL (Fig. 4Ba'-d'). Besides, Tcf activity is partly overlapping with *barhl1* expression domain (Fig. 4Bc", c'"-d").

We next assessed the impact of Barhl1 GOF and LOF on Tcf activity (Fig. 4C). Whereas *mBarhl1* overexpression decreased Tcf activity (Fig. 4Ca), we observed a threefold increase in Tcf activity upon Barhl1 downregulation with *MObarhl1-1* (Fig. 4Cb,c). In contrast, *MOct* had no effect on Tcf activity (Fig. S4A). We further inhibited Barhl1 by selective knock-out (KO) of *xbarhl1* gene in the pbin7LefdGFP line (F0 generation) using Crispr/Cas9 genome editing technology (Fig. S4B). We observed that Barhl1 KO induced an average twofold increase in Tcf transcriptional activity (Fig. 4Da-c). We assessed phenotypic penetrance in Crispr/Cas9 injected embryos. We observed different levels of phenotypic severities in >70% of injected embryos, ranging from a slight increase in Tcf activity observed in ~20% of injected embryos to >40% of injected embryos exhibiting strong to complete penetrance as observed by a significant increase in Tcf activity in R1 (Fig. 4d).

To determine whether Barhl1 effects were mediated through its interaction with Gro, we used an inducible form of *mBarhl2-EHsGR, which* contains the two EH1 domains of Barhl2 (Fig. S2), and has been demonstrated to act as a dominant negative for Tcf repressive activity by competing for Gro binding (Sena et al., 2019a). Overexpression of *mBarhl2EHsGR* induced a phenotype similar to that of Barhl1-KD, an increase of the URL/EGL size at the expense of GNP commitment/differentiation (Fig. 4Ea, b; S4).

In conclusion, Barhl1 directly interacts with Tcf and Gro, and normally limits Tcf transcriptional activity in the cerebellar primordium.

Partly through its limiting of Tcf transcriptional activity, Barhl1 allows GNP to exit the proliferating URL

The URL germinative zone is characterized by its proliferative state, and its bordering of the roof plate. We asked whether the enlargement of the URL/EGL territories observed in Barhl1-KD tadpoles was corroborated with an increased proliferation in the URL and/or within the EGL. Using immunofluorescence staining for Phosphorylated-Histone H3 (PHH3), a marker of cells undergoing mitosis, we followed proliferation in tadpoles injected with either *MOct* or *MObarhl1-1* at stage 45 and 48.

In *MOct* injected tadpoles, PHH3+ cells were solely detected within the URL (Fig. 5Aa) (Butts et al., 2014). In contrast, we observed changes in the PHH3+ cells pattern in Barhl1-KD embryos, including a 1.2-fold lengthening of the URL on the injected side relative to the control side at both stage 45 and 48, associated with presence of PHH3+ cells within the cerebellar plate (Fig. 5Ac-e). Because it was morphologically easier to distinguish the URL from the VZ at stage 48, we performed our following analysis at this later developmental stage (Fig. 5Ab). We measured an average 2-fold increase in the number of PHH3+ cells on the injected side compared to the control side (Fig. 5Ac, d, f), and quantified the presence of ectopic proliferating cells in the cerebellar plate (Fig. 5Ac, d, g).

We next investigated whether Tcf inhibition counteracted Barhl1-KD effect on URL lengthening using ISH for *nmyc*, a marker of both the URL and the R1 caudal boundary (Fig. 5B). As previously observed, Barhl1-KD increased the URL length, whereas *tcf7l1-Δβcat-GR* overexpression reduced it (Fig. 5Ba-c, f). However, co-injection of *MObarhl1-1* and *tcf7l1-Δβcat-GR* mRNA brought back the URL size to normal (Fig. 5Bd-f).

In conclusion, Barhl1-KD cells are compromised in both their ability to leave the URL niche, and to become postmitotic. Barhl1-KD defects are at least partly due to over-activation of Tcf.

Analysis of R1 Barhl1 KD transcriptomic analysis reveals an increase in Tcf activity and some *hes/hey* genes expression, an increase in markers of neural stemness, and a decrease in neural differentiation

To further document Barhl1 URL activity, we designed an RNA-sequencing experiment allowing the identification of Barhl1 direct and indirect target genes in the early *Xenopus* cerebellum. We isolated and sequenced RNA from dissected stage 42 R1 tadpoles injected with *MObarhl1-1*, *MObarhl1-2* or *MOct*. Samples were compared through differential expression (DE) analysis (Fig. S5)(Table S1-S3). Principal component analysis of these R1 samples demonstrated that they clustered by Barhl1-KD status (Fig. S5B), indicating that changes in gene transcription were consistent across different clutches. We identified 1622 and 830 differentially expressed genes between respectively *MObarhl1-1* and *MObarhl1-2* injected R1, compared with *MOct* injected R1, with 575 DE genes common between MOs injected samples (Fig. S5C, D). A heatmap (Fig. 6A), and Volcano plots (Fig. 6B) representing upregulated and downregulated DEG for both MOs, are shown. Using the clusterProfiler algorithm (Wu et al., 2021) we performed gene ontology analysis (GO), and compared altered biological functions between both Barhl1-KD conditions (Fig. 6C, D). This GO analysis reveals that the most significantly upregulated genes acted as transcriptional activators (Fig. 6C), while the downregulated DEG are involved in neuronal differentiation (Fig. 6D).

We next investigated the presence of Barhl1 Cis Regulatory Motifs (CRM) defined as CAATTAC/G and its mirror motif (Chellappa et al., 2008), within the regulatory sequences - 5Kb and 30kb upstream or downstream of the Transcription Start Site (TSS) - of previously identified DEG common to *MObarhl1-1* and *MObarhl1-2* conditions. For 5Kb we observed 71% of DEG regulatory regions contain at least 1 Barhl1 CRM, while 34% contain 2 or more Barhl1 CRM (Fig. 6E, Fig. S5, Table S4). For 30kb all DEG regulatory regions contain at least 2 Barhl1 CRM, 87.5% contain 5 or more Barhl1 CRM and 33% 10 or more Barhl1 CRM (Fig. 6E, Table S5). To investigate which Barhl1 target genes are also regulated by TCF we similarly searched for TCF CRM defined as CTTTGAA/CTTTGAT, within the regulatory sequences of previously identified DEG common to *MObarhl1-1* and *MObarhl1-2* (Kjolby et al., 2019; Nakamura et al., 2016). We observed that 76% of Barhl1 depleted DEG regulatory regions contain at least one Tcf CRM: 26% contain one CRM, 49% contain at least two Tcf CRM (Fig. 6E, Fig. S5, Table S6). In agreement with our functional data, amongst the Barhl1-KD DEG we observed an upregulation of *sp5,* a bona fide direct target genes of TCF (Fig. 6A,B; Table S1-S3) (Wu et al., 2012). We also observed an upregulation of Wnt Ligand Secretion Mediator (*wls*), a URL marker (Yeung et al., 2014) (Fig. 6A,B; Table S1-S3). Of note whereas both *wnt2b* and *wnt8b* are upregulated by Barhl1 KD their expression levels are very low in the cerebellar anlage (Fig. S5E; Table S1-S3). Thereby Barhl1 depletion activates Tcf activity throughout the cerebellar anlage, specifically within the URL and the cerebellar plate.

Amongst the DEG, we also observed an upregulation of *hes5* family genes (*hes5.1, hes5.2, hes5.3, hes5.4*), and HES/HEY-Like TF (*helt*) *(*also known as *Heslike and Megane),* which are downstream effectors in the Notch pathway (reviewed in Kobayashi and Kageyama, 2014). We also observed a down regulation of the Delta/Notch-like epidermal growth factor (EGF)-related receptor (*dner*), which has been suggested to be a neuron-specific Notch ligand (Eiraku et al., 2005) that inhibits neural proliferation and induces neural and glial differentiation (Hsieh et al., 2013). Using ISH, we validated a cerebellar upregulated expression for *hes5.1* in the EGL (Fig. 6Ga,d). We further asked whether *hes5.*1 upregulation observed in Barhl1

morphants depended on Notch signaling. MOBarhl1 injected tadpoles were grown either in carrier, or in LY411575, a potent inhibitor of γ-secretase that is strictly necessary for intracellular transmission of Notch signals (Belmonte-Mateos et al., 2023). As expected LY411575 induced a down regulation of *hes5.1* expression levels within the cerebellum (Fig. 6Ge)(Jacobs and Huang, 2019; Myers et al., 2014). However, despite γ-secretase inhibition, Barhl1 depletion upregulated *hes5.1* expression (Fig. 6Gb-d).

Our differential expression dataset also reveals that genes that are the most up-regulated in the Barhl1 KD conditions are involved in adult neural stem cell (NSC) maintenance. For example, *dmrta2* that encode for doublesex and mab-3-related TF a2, also known as *dmrt5,* the orphan nuclear receptor subfamily 2 group E member 1 (*nr2e1*) commonly known as Tailless (Tlx), and *zic3,* a member of the Zinc Finger of the Cerebellum (Zic) family known to be involved in regulation of neuronal progenitor proliferation versus differentiation, and cerebellar patterning (reviewed in Aruga, 2004; Aruga and Millen, 2018; Houtmeyers et al., 2013) are all upregulated (Fig. 6A,B; Table S1-S3). Using ISH, we validated a cerebellar upregulated expression for *zic3*, which transcripts are present in the URL, and *otx2* that is detected in a subset of GNP at stage 41-42 (Fig. 6Gd; Fig. S5F).

Finally, in agreement with our functional data, the Basic Helix-Loop-Helix Family Member E22 (*bhlhe2*), a downstream target of Neuro-D1 , is downregulated in Barhl1 depleted R1 (Ma et al., 2022) (Fig. 6A; Fig. S5E; Table S1-S3).

Taken together, our transcriptomic analysis identifies direct and indirect Barhl1 target genes, and confirms our functional data. Our *in silico* search of Barhl1 target genes regulatory regions further validates that Barhl1 partly acts by inhibiting Tcf transcriptional activity. Our data also argue that Barhl1 directly or indirectly inhibits expression of *hes5* genes independently of Notch signalling.

DISCUSSION

This study, conducted in amphibian, establishes that i) Tcf transcriptional activity appears necessary for inducing both *atoh1* expression, and the cerebellar URL; ii) a role for *hes4/5* genes in the EGL that is independent of proliferation; iii) Barhl1 is necessary for URL cells exit from their niche, partly through direct repression of Tcf transcriptional activity; iv) Barhl1 KD maintains GNP in a non-proliferative, immature state while increasing both Tcf activity and *hes5* expression. Similarly in amniotes, Tcf activity is detected in the URL and switched off in the EGL. Notch target genes, and Barhl1/2, transcripts are detected in the amniotes URL and EGL. Taken together, these observations argue for a conserved role of a Barhl in maintenance of the URL/EGL germinative niche via Tcf and potentially *hes/hey* genes regulation.

GN development in *Xenopus* is similar to that of higher vertebrate

Our data provide a developmental map of GNP development in *Xenopus*, revealing that the processes leading to the emergence of URL derivatives and maturation of GN are similar to those seen in higher vertebrate (Gona, 1972; Herrick, 1914) (reviewed in Hibi et al., 2017; Miyashita and Hoshino, 2022). Our analysis confirms the absence of proliferating cells within the EGL (Butts et al., 2014), and shows EGL expression of *hes5* and *hes4,* markers of stem/progenitor cells. Our data argue that, at least in amphibians, *hes* genes are involved in maintaining GNP in an immature state, independently of proliferation.

In the cerebellar primordium Tcf transcriptional activity appears necessary for *atoh1* expression and URL induction

Our data indicate that Tcf transcriptional activity is necessary for induction of *atoh1* expression, and of the URL territory. Studies performed in mouse neuroblastoma, and neural progenitor cells in culture, identified two TCF/LEF binding sites in the 3' enhancer region of *Atoh1* required for *Atoh1* activation (Shi et al., 2010). In these cells, the concomitant inhibition of Notch signaling and activation of WNT/TCF, is required for *Atoh1* expression (Shi et al., 2010). In mice low levels of Notch activity are necessary to induce a URL fate (Khouri-Farah et al., 2022; Zhang et al., 2021). These data argue that concomitant TCF activation and Notch inhibition are responsible for *Atoh1* URL induction. Once activated ATOH1 directly induces its own expression, which maintains the URL territory (Klisch et al., 2011).

Both *tcf7l1* and *tcf7* transcripts are detected in the amphibian cerebellar anlage and could mediate Wnt signaling in this germinative niche. Of note Wnt canonical ligands present in the MHB like Wnt1, and in the roof plate, specifically Wnt3 and Wnt3a, may participate to Tcf activation within the URL (Fig. S5E) (Roelink and Nusse, 1991). Whether Tcf is activated in a Wnt-dependent manner in the URL at the analyzed stage has not been proven.

Three of the four Tcf isoforms (Tcf7l2, Tcf7 and Lef1), mostly act as transcriptional activators, whereas the fourth (Tcf7l1) mostly acts as a transcriptional repressor (Liu et al, 2005)(reviewed in Arce et al., 2006). Transcriptomic analyses of human cerebellar development reveal that the transcriptional activator TCF7 is active in the human URL (Aldinger et al., 2021), whereas Tcf7l2 is detected in the mouse URL (Carter et al., 2018). In both species, Tcf7l1 is associated with differentiated GNs (Aldinger et al., 2021; Wizeman et al., 2019). Thereby our findings in amphibian are relevant for amniotes URL biology.

In the URL, Barhl1 promotes GNP exit from their germinative niche and their progression towards differentiation at least partly through Tcf inhibition

Barhl1 depletion and Knock-Out dramatically increases Tcf transcriptional activity in the URL/EGL. Both the increase in URL length, and the delay in GNP commitment/differentiation induced by Barhl1 depletion, are fully compensated by co-expression of a constitutive inhibitory form of Tcf7l1. Our R1 transcriptomic analysis of Barhl1-KD embryos reveals an increase of Tcf activity. 75% of Barhl1 depleted DEG regulatory regions contain at least one Tcf CRM. These include markers of the URL and EGL, and *wls* which in mice has been described to orchestrate cerebellum development (Yeung and Goldowitz, 2017; Yeung et al., 2014). Barhl1 KD significant upregulated genes act either by regulating the fine equilibrium between a proliferative state and commitment and / or in maintenance of their stem/progenitor features. In rodents, *dmrta2* (*dmrt5)* expression maintains NSC self-renewing ability and is transcriptionally regulated by TCF (Konno et al., 2012; Young et al., 2017). The primary function of the orphan nuclear receptor *Nr2e1* (also known as *Tlx*) is to maintain NSC pools in an undifferentiated, self-renewing state (Kandel et al., 2022) (reviewed in Islam and Zhang, 2015; Wang et al., 2013). *otx2* expression is associated with GNP high proliferation rate (El Nagar et al., 2018; Fossat et al., 2006), and *zic3* is involved in maintaining pluripotency in both ESC (Lim et al., 2007; Lim et al., 2010), and neural progenitor cells (Inoue et al., 2007). Finally, most downregulated DEG are involved in terminal neuronal differentiation including *Bhlhe2*, which in mice is a regulator of post-mitotic GN radial migration towards the IGL (Ma et al., 2022; Ramirez et al., 2021).

The current model of Wnt canonical pathway activation is that β-Catenin promotes transcription of Wnt-responsive gene by either displacing Gro (Daniels and Weis, 2005; Roose et al., 1998), or by displacing the whole Tcf7l1-Gro repressor complex and replacing it with an activator complex containing β-Catenin in association with Tcf7 (Hikasa et al., 2010; Roël et al., 2002). Importantly, this switch from repression to activation of transcription for canonical Wnt pathway target genes depend on the stability of the Tcf7l1-Gro repressor complex, which promotes compaction of chromatin when the Wnt/β-Catenin pathway is switched off (Shy et al., 2013). We propose that, in the amphibian cerebellar URL, activation of either Tcf7 and/or Tcf7l1, participate to *atoh1* expression and initiates GNP developmental program. A gradient of GNP differentiation initiated in the caudal R1 and progressing to R1 rostral part is established. Once activated Atoh1 directly induces *barhl1* transcription in a caudal R1 URL subpopulation (Kawauchi and Saito, 2008; Klisch et al., 2011). There, Barhl1 binds to Tcf7l1 and/or Tcf7 thereby preventing their further activation, and switching off the GNP "URL" program. GNP then move out of the URL and progress towards commitment and differentiation. Barhl1 role in GNP development, through its inhibiting of Tcf activity, is similar to Barhl2 activity during Spemann organizer formation (Sena et al., 2019). *in silico* analysis performed on active medulloblastoma enhancers, together with our previous study on Barhl2, indicate that Barhl1 and Barhl2 have long-range activity via their specific binding on DNA perhaps on super-enhancers, and via chromatin modifications (Lin et al., 2016; Sena et al., 2019). Indeed, all DEG containing TCF CRM also contain at least two Barhl1 CRM 30kb upstream or downstream of their TSS. A more thorough study is necessary to understand how Tcf and Barhl1 interact *in vivo,* and regulate transcription within the cerebellar primordium. Of note our study does not differentiate gene regulation by Barhl1 alone, or via its interaction with Tcf.

Barhl1 inhibits *hes/helt* transcription in the cerebellar primordium

Depletion of Barhl1 also leads to a significant upregulation of *hes5* isoforms and *helt,* which all directly repress proneural genes expression (Ables et al., 2011; Alunni and Bally-Cuif, 2016;

Giachino and Taylor, 2014; Imayoshi et al., 2010; Kageyama et al., 2019; Lampada and Taylor, 2023). Importantly γ-secretase inhibition in Barhl1 morphants does not prevents *hes5* upregulation. Gro/TLE, the main corepressor partner of Tcf, also participates to Notch signaling (reviewed in Bou-Rouphael and Durand, 2021; Cinnamon et al., 2008). Taken together our results argue that within the cerebellar anlage Barhl1 transcriptionally inhibits *hes5/helt* independently of Notch signaling, maybe via the recruitment of a protein complex containing Gro/Tle. Of note *Hes5* is not expressed in rodent EGL (Khouri-Farah et al., 2022), and *Hes4,* a marker of stemness in *Xenopus* (El Yakoubi et al., 2012), is not expressed in mice, while its expression is found in Human. Whether, in amniotes a HES related protein maintains some GNP in an immature state remains to be investigated.

Barhl in amphibian versus amniote GNP development

In rodents, ATOH1 directly induces the expression of both *Barhl1* and *Barhl2* (Kawauchi and Saito, 2008; Klisch et al., 2011). scRNA-sequencing analysis of mouse cerebellar *Atoh1* lineage cells reveals that *Barhl1* is associated with early stages of GNP differentiation, whereas *Barhl2* expression is uniquely associated with early fate commitment (Carter et al., 2018). *Barhl1* and *Barhl2* are highly conserved through evolution (reviewed in Bou-Rouphael and Durand, 2021). Their functional conservation is evidenced through studies in various species, including mouse, *C. elegans* and the acorn worm *Saccoglossus kowalevskii* (Schwartz and Horvitz, 2007; Yao et al., 2016). Mice carrying a knock-out (KO) insertion within the mouse *Barhl2* coding frame die before P24 following among other signs, defective weight gain and impaired motor coordination, reflecting cerebellar deficiency (Ding et al., 2009). Whereas a role for one of the Barhl TF in emergence and maintenance of the amniote's URL germinative niche is predictable, Barhl2 appears as a more suitable candidate than Barhl1 for this function.

ACKNOWLEDGEMENTS

The authors gratefully acknowledge M. Perron, D. Turner, P. Kreig, J. Christian, R. Vignali and G. Schlosser, P. Walentek, S. Hoppler and M. Salonna for gifts of materials. We thank the IBPS Aquatic platform supported by Sorbonne Université, CNRS, IBISA and the Conseil Régional Ile-de-France, specifically S. Authier and M. Abdelkrim, for Xenopus care. We thank C. Antoniewski (ArtBio platform, FR3631 IBPS) for tutoring in RNAseq data analysis and the team of G. Almouzni (Institut Curie) for providing high sensitivity RNA screentape system. We acknowledge Ann Lohof and Rachel Sherrard for editing work on the manuscript. We thank A. El Helou for technical help. This work was supported by the Centre National de la Recherche Scientifique (CNRS - UMR7622), donors to B Durand project, Sorbonne-Université, the Ligue Nationale contre le Cancer Comité Ile de France (RS19/75-52 and RS23/75-68). The CNRS supports Béatrice Durand and Mohamed Doulazmi. Alexis Eschstruth is supported by Sorbonne Université, Johnny Bou-Rouphael by a fellowship from the “Ministère de la Recherche”, A. Abdou by CNRS funds.

AUTHOR CONTRIBUTIONS

Conceptualization, J.BR., and B.C.D.; Methodology, J.BR., M.D., A.E., A.A. and B.D., Software, M.D.; Investigation, J.BR., M.D., A.E., and B.C.D.; Data curation, J.BR., and M.D., Writing – Original Draft, J.BR., and B.C.D.; Writing — Review & Editing, J.BR., M.D., A.E., A.A and B.C.D.; Visualisation, J.BR., and B.C.D.; Funding Acquisition, B.C.D.; Resources, J.BR., M.D., A.E., A.A. and B.C.D.; Supervision, B.C.D.;

DECLARATION OF INTERESTS

The authors declare no competing interests.

MATERIALS and METHODS

EXPERIMENTAL MODEL

Xenopus embryos care and husbandry

X. laevis embryos were obtained by conventional methods of hormone-induced egg laying and *in vitro* fertilization and were staged according to (Nieuwkoop and Faber, 1994). *X. tropicalis* transgenic Wnt reporter pbin7LefdGFP has been generated as previously described (Borday et al., 2018; Tran and Vleminckx, 2014; Tran et al., 2010). Briefly, the synthetic Wnt-responsive promoter consists of 7 copies of TCF/LEF1 binding sites and a TATA box driving destabilized green fluorescent protein (eGFP) and a polyA sequence. *gfp* expression reveals Wnt/TCF activity. *X. tropicalis* embryos were obtained by *in vitro* fertilization. Experimental procedures were specifically approved by the ethics committee of the Institut de Biologie Paris Seine (IBPS) (Authorization 2020-22727 given by CEEA #005) and have been carried out in strict accordance with the European community directive guidelines (2010/63/UE). B.D. carries the authorization for vertebrates' experimental use N°75-1548.

METHOD DETAILS

Plasmids design and preparation

mbarhl1-HA-GR contains the full-length *mbarhl1* sequence (two Engrailed-Homology (EH1) motifs, Nuclear Localization Signal (NLS); Homeodomain HD); and the C-terminal part), followed by an HA tag at the C-terminal part. This construct is inducible as it contains a glucocorticoid receptor which can be activated by dexamethasone (10uM). Dexamethasone-inducible *mbarhl2-EHs-GR* contains the first 182 amino acids (a.a) of mouse Barhl2 full-length cDNA, which correspond to the N-terminal EHs Gro-binding domains, and has been shown to act as a dominant negative (Sena et al., 2019). The full-length *mbarhl1-HA-GR* and truncated *mbarhl2-EHs-GR* constructs were generated in pCS2+ by Vector Builder. Non-inducible *mbarhl1-Myc* and *xbarhl1-Flag* were generated by GeneScript. Peptide sequences of the tags used are the following: HA (YPYDVPDYA); FLAG (DYKDDDDK) and MYC (EQKLISEEDL). The constitutive repressor pCS2-Tcf7l1-ΔβCat-GR was a gift from H. Clevers (Molenaar et al., 1996), and consists of the full-length Tcf7l1 lacking the β-catenin-binding domain (BCBD), which reinforces its repressive activity. Constructs used for immunoprecipitation assay are *pCS2+ mbarhl1-3xFlag-HA* which was generated by Vector Builder. It contains the full-length *mbarhl1* sequence followed by three Flag tags and one HA tag at the C-terminal part. *pCS2+ Myc-Tcf7l1, pCS2+ Myc-Tcf7l2, pCS2+ Myc-Tcf7, pCS2+ Flag-Gro4* and *pCS2+GroHA* have been previously described (Liu et al., 2005; Sena et al., 2019). All necessary sequences were obtained from NCBI database. Constructs were validated by western blot on extracts from injected embryos or cell lysates.

mRNA synthesis, morpholino oligonucleotides (MOs) and *Xenopus* injection

Capped messenger RNAs (mRNAs) were synthesized using the mMessage mMachine kit (Invitrogen) and resuspended in RNAse-free water. Antisense morpholino oligonucleotides (MOs) were generated by Gene Tools. ATG start-site *MObarhl1-1* and *MObarhl1-2* were designed to block initiation of xBarhl1 protein translation. The MO were designed in a region overlapping the translation initiation site, so that they do not recognize mouse *Barhl1* or *xbarhl2*

mRNA (Fig. S3). To establish the specificity of the MO effect, we tested the ability of *MObarhl1-1* and *MObarhl1-2* to specifically inhibit translation of *xbarhl1* mRNA. Flag-tagged *xbarhl1* (*xbarhl1-flag)* or myc-tagged *mBarhl1* (*mBarhl1-myc*) were co-injected with *MObarhl1-1*, or *MObarhl1-2*, or a control MO (*MOct*) (Fig. S2). Western blot analysis on extracts from injected embryos confirmed a *MObarhl1*-mediated dramatic decrease in *Xenopus* Barhl1 protein levels, while MOct had no effect. We also observed that *MObarhl1-1* did not decrease mBarhl1-myc protein levels (Fig. S2; S3). *MObarhl1-1* was used for both *X. laevis* and *X. tropicalis* as the mRNA sequence of *barhl1* is highly conserved between both species, more specifically in the region on which *MObarhl1* is hybridized. Standard control MO from gene tools was used in this study. MO sequences and doses are summarized in Table 2.

Xenopus embryos were injected unilaterally in one dorsal blastomere at the four and eight-cell stage together with *gfp* as a tracer for phenotype analysis by *in situ* hybridizations (ISH), except for CRISPR/Cas9 genome editing and RNAseq analysis *(see corresponding sections in material and methods)*. MOs were heated for 10 min at 65°C before usage. Injected embryos were transferred into 3% Ficoll in 0.3X Marc's Modified Ringer's (MMR) buffer (stock solution: 1M NaCl, 20 mM KCl, 20 mM $CaCl_2$, 10 mM $MgCl_2$, 50 mM HEPES pH 7.4). 10nl of mRNA or MO solution was injected together with a tracer in *X. laevis* while 5nl were injected in *X. tropicalis*. In *X. laevis*, MOs or mRNAs were co-injected with *gfp* mRNA (100 pg). MOs or mRNAs were co-injected with *mcherry* (100 pg) in *X. tropicalis.* Concentration of injected mRNA and MOs per embryo have been optimized in preliminary experiments. The minimal mRNA or MO quantity that induced the specific phenotype without showing toxicity effects was used. For embryos injected with inducible constructs, half of the injected embryos were treated with 10µM dexamethasone at stage 35/36 while the other half were left untreated and served as control. All necessary *Xenopus* sequences were obtained from Xenbase.

in situ **hybridization**

Embryos were staged according to (Nieuwkoop and Faber, 1994), and collected at the desired stage, then fixed in PFA4% for 1-2 hours at room temperature and dehydrated in 100% MeOH. ISH were performed using digoxigenin (DIG)-labeled probes. Antisense RNA probes were generated for the following transcripts: *atoh1, barhl1, hes4, hes5.1, neurod1, pax6, n-myc, otx2, tcf7l1, tcf7l2, tcf7, lef1, zic3, wnt2b, wnt8b* and *gfp* according to the manufacturer's instructions (RNA Labeling Mix, Roche). pCS2-Gfp is a gift from David Turner (University of Michigan, Ann Arbor, MI, USA). pBSK+xBarhl1 is a gift from Roberto Vignali (Unità di Biologia Cellulare e dello Sviluppo, Pisa Italy). pCS2-Atoh1 is a gift from G. Schlosser (University of Galway, Ireland). pBSK+Wnt2b was a gift from S. Sokol (Icahn School of Medicine at Mount Sinai, NY, USA). pBSK+Wnt8b was a gift from J Christian (University of Utah, USA). Tcf isoforms in pCS2 were provided by S Hoppler. ISH was processed following the protocol described by (El Yakoubi et al., 2012; Sena et al., 2019). barhl1 and barhl2 reagents are available upon request. DISH was processed as described by (Juraver-Geslin et al., 2014). For *X. laevis* embryos, following rehydration, the eyes and ectoderm overlying the anterior neural tube were removed, which allows to skip the further Proteinase K (PK) treatment. Dissections weren't performed on *X. tropicalis* embryos which were treated with PK. In both cases, bleaching was carried out, and samples were incubated with the probes overnight. Alkaline phosphatase-conjugated anti-DIG or anti-FLUO antibodies (Roche) were incubated 3 hours at room temperature. Enzymatic activity was revealed using NBT/BCIP (blue staining) and INT/BCIP (red staining) substrates (Roche). Following ISH, post-fixation was

carried out in PFA 4% and the neural tubes of control and injected *X. laevis* embryos were dissected in PBS-0.1% Tween and stored in 90% glycerol. *X. tropicalis* embryos were stored in PFA 4%. Dissected neural tubes or embryos were photographed on a Leica M165 FC microscope equipped with Leica DFC320 camera using the same settings to allow direct comparison. Dorsal and lateral views of the dissected neural tubes were photographed.

Pharmacological treatment

Embryos were treated either with 25 µM of the gamma-secretase inhibitor LY411575 (Sigma-Aldrich) or DMSO for control, added to *Xenopus* culture environment for 24 h.

Immunofluorescence

Immunofluorescence was carried out as previously described (Juraver-Geslin et al., 2011). The entire brains of wild-type (WT) and MO-injected *X. laevis* embryos were carefully dissected and transferred into a tube containing PBS-0.1% Tween, where they were progressively permeabilized. Samples were incubated with primary antibody (anti-Phospho-Histone H3; Upstate Biotechnology Cat#06–570; d1:500) at 4°C overnight. Cellular nuclei were stained with BisBenzimide (BB) (Sigma) which was added to the solution containing diluted secondary antibody (Alexa Fluor 488 donkey anti-rabbit IgG; Invitrogen; d1:500) and incubated at 4°C overnight. Neural tubes were captured on a Zeiss Axio Observer.Z1 microscope equipped with apotome. Acquisitions were taken using the Z stack tool from the most superficial layer to deeper layers.

Immunoprecipitation in transfected HEK293T cells

HEK293T cells were originally obtained from ATCC (CRL-3216), verified to be free of mycoplasm and cultured in supplemented Dulbecco's modified Eagle's medium (DMEM) (Gibco). Cells were transfected with expression vectors for *pCS2-mbarhl1-3xFlag-HA; pCS2-mbarhl1-Myc; pCS2-Tcf7l1-Myc; pCS2-Tcf7l2-Myc; pCS2-Tcf7-Myc pCS2-Gro-Flag and pCS2-Gro-HA* (gifts from S. Hoppler or available upon request) encoding tagged proteins using the Phosphate Calcium method. Plasmids coding for pCS2+ or pSK+ were used as a supplement to ensure that cells in different dishes were transfected with the same quantity of expression vectors and plasmids (a total of 2 µg). Thirty-six hours post-transfection, cells were harvested and lysed in ice-cold lysis buffer (20 mM Tris pH7.6, 150 mM NaCl, 1% Triton, 1 mM EDTA) supplemented with completeTM protease inhibitor (Roche). Cell lysates were centrifuged 15min at 14,000 rpm. Protein complexes were precipitated from the cell lysates with anti-c-Myc antibody (clone 9E10). Protein complexes were then precipitated with protein A-Sepharose beads (Sigma) pre-washed with lysis buffer. Immunoprecipitated proteins were eluted from protein A beads by heating beads in Laemmli sample loading buffer (BioRad).

Western blot

Western blot (WB) analysis was performed on protein extracts from injected/WT *Xenopus* embryos, and on extracts from transfected HEK923T cells. *Xenopus* embryos were injected with *mbarhl1HAGR, xbarhl1Flag, mBarhl1Myc, mBarhl2EHsGR* mRNA at the two-cells stage, targeting both blastomeres. Proteins were extracted at stage 10 with lysis buffer (10 mM Tris-HCl pH 7.5, 100 mM NaCl, 0.5%NP40, 5mM EDTA supplemented with a cocktail of protein

inhibitors). WB was carried out using the conventional methods. Proteins were separated by 10% SDS-polyacrylamide gel and transferred to nitrocellulose membrane. Membranes were blocked using 5% milk and incubated with the corresponding primary and secondary antibodies diluted in 5% milk (summarized in tables 3 and 4). Proteins were detected with Western Lightning Plus-ECL (Perkin Elmer Life Sciences). Membrane stripping was carried out between two staining steps using stripping buffer (Thermo Scientific) for the removal of primary and secondary antibodies from the membranes. ChemiDoc MP Imaging System (BioRad) was used for imaging the blots.

CRISPR/Cas9

Three CRISPR target sites (*barhl1-1* : GAGTCGGACGAGGCCATGGAAGG), *barhl1-2* : ACCAGCTCTGTGCGACAGAATGG, *barhl1-3* : AGAGTTGGACTCCGGGCTGGAGG) cutting respectively at 2, 37 and 230 bp from the beginning of the coding sequence were selected for their high predicted specificity and efficiency using CRISPOR online tool (http://crispor.tefor.net/). Alt-R crRNA and tracrRNA were purchased from Integrated DNA Technologies (IDT, Coralville, IA, USA) and dissolved in duplex buffer (IDT) at 100µM each. cr:tracrRNA duplexes were obtained by mixing equal amount of crRNA and tracrRNA, heating at 95°C for five minutes and letting cool down to room temperature. gRNA:Cas9 RNP complex was obtained by incubating 1µL 30µM Cas9 protein (kindly provided by TACGENE, Paris, France) with 2µL cr:tracrRNA duplex in a final volume of 10 µL of 20mM Hepes-NaOH ph 7.5, 150mM KCl for 10 min at 28°C. *X. tropicalis* one-cell stage embryos were injected with 2nL of gRNA:Cas9 RNP complex solution and were cultured to the desired stage. For coinjection, the three complexes were mixed at equal quantity.
Single embryo genomic DNA was obtained by digesting for 1h at 55°C in 100 µL lysis buffer (100 mM Tris-Hcl pH 7.5, 1 mM EDTA, 250 mM NaCl, 0.2% SDS, 0.1 µg/µL Proteinase K), precipitating with 1 volume of isopropanol and resuspended in 100µL PCR-grade water. The region surrounding the sgRNA binding sites was amplified by PCR using *X. tropicalis Xt_barhl1_F* (CAGCTCCTCCGACTTTTGTG) as forward primer and *Xt_barhl1_R* (GTTGCCCGTTGCTGGAATAA) as reverse primer. CRISPR efficiency was assessed by T7E1 test (Mashal et al., 1995) on mono-injected embryos and by detecting deleted fragments on coinjected embryos.

RNA-sequencing and data analysis

X. laevis embryos were injected with three different conditions: *MObarhl1-1*; *MObarhl1-2* and *MOct* in the two dorsal blastomeres at four cells stage. At stage 42, neural tubes were extracted in RNAse-free conditions, and the rhombomere 1 which includes the URL was carefully dissected. For each condition, three biological replicates were collected. Each replicate contains three rhombomeres, which was the optimal number to get the minimal RNA concentration required for this experiment (Total RNA concentration was ~30ng per sample). Briefly, total RNA was extracted using the TRIzol reagent (ambion) according to the manufacturer's instructions. The overall RNA quality was assessed using Agilent High Sensitivity RNA ScreenTape System. Samples with an RNA Integrity Number (RIN) > 9 were used for subsequent analysis. Poly A RNA was purified. Sequencing was performed using Illumina NovaSeq (paired-end sequencing) by Next Generation Sequencing Platform (NGS) (Institut Curie). RNAseq data processing was performed using Galaxy server of ARTBio platform (IBPS). The raw data base of our RNA sequencing data and a brief description of

method is accessible on https://www.ebi.ac.uk/ena/browser/view/PRJEB64149, secondary accession ERP149284, title: role of barhl1 in the amphibian cerebellum.

Data sets were aligned against the *X. laevis* v10.1 genome assembly downloaded with its corresponding annotation file from Xenbase (Fortriede et al., 2020). Alignment was made using two read mapping programs, STAR v2.7.8a (Dobin et al., 2013) and HISAT2 v2.2.1 (Kim et al., 2015). Quality control checks were assessed using FastQC v0.73 (Andrews, 2010) and summarized in a single report generated by MultiQC v1.9 (Ewels et al., 2016). As both alignment programs provided comparable results, we proceeded with STAR alignment tool. The number of aligned reads was counted by featurecounts tool v2.0.1 (Liao et al., 2014). Finally, we used the DESeq2 v2.11.40.6 package (Love et al., 2014) to determine differentially expressed genes (DEG) from count tables. In the present study, genes with adjusted p value pAdj<0.001 were selected as significant DEG. Venn diagrams were produced with JVenn v2021.05.12 (Bardou). Volcano Plots v0.0.5 were generated to show significant upregulated and downregulated genes, only a selection of DEG names were represented.

Further analysis and data visualization were performed using R v4.2.1package. A heatmap was generated to visualize gene expression across the samples. To overcome the lack of *Xenopus* gene ontology (GO) annotation, we replaced *X. laevis* gene symbols with the Human orthologs. Functional enrichment analysis was performed using the *compareCluster* function of ClusterProfiler v4.8.1 [56] to identify GO-term enrichment amongst DEG with pAdj<0.001 as threshold. It provides the biological processes, cellular components, and molecular functions of DEG and compares each of the three subgroups between both knockdown conditions.

QUANTIFICATION AND STATISTICAL ANALYSIS

Image processing and analysis

For ISH performed on embryos injected unilaterally, comparison of the expression levels between injected and control sides was assessed using a specific macro from ImageJ v2.1.0/1.53c (Abràmoff et al., 2004; Schneider et al., 2012). The macro functions based on the RGB color mode. RGB images are split into three channels (red, green, and blue) and pixel values corresponding only to the blue channel are recorded, excluding the red and green channels, since the signal recorded on the blue channel represents the expression levels. For each image, the region of interest (ROI) was specified, and its dimensions were fixed, such that the same ROI is placed on the control and injected side of the embryo which prevents any subjectivity in ROI determination. Measured are the area corresponding to the blue signal; the mean or average value of signal within the selected ROI; and the integrated density which is the equivalent of the product of area and mean, as it sums the values of pixels in the selection. In this study, ratio of integrated density measured in the injected *versus* control side was assessed. The macro is available from the authors upon request and will be available as a plug-in in ImageJ.

The same macro was used for the analysis of CRISPR/Cas9-injected embryos, except that ROI was placed in all the rhombomere 1 as the entire embryo was targeted. The mean of int. density values of control embryos was compared to each individual int. density value of control

and injected embryo. Phenotype penetrance was evaluated by counting and classifying embryos based on the intensity of *gfp* expression increase.

For immunofluorescence, Z-stack images were reconstructed and processed using ImageJ v2.1.0/1.53c. PHH3-positive cells were counted, and the length of the RL was measured on the control and injected side. Ratio of PHH3-positive cells and RL length in the injected *versus* control side was measured.

For the same experiment, all images were acquired using the same magnification and camera settings. In this way, all images were processed in a standardized manner, such that results are objectively analyzed. Final images were processed with Adobe Photoshop (v24.00).

Statistical analysis

Three independent experiments were performed for each condition analyzed. Dissected neural tubes and embryos were analyzed individually, and the results were pooled for data representation. Statistical analyses were implemented with R. Normality in the variable distributions was assessed by the Shapiro-Wilk test. Furthermore, the Levene test was performed to probe homogeneity of variances across groups. Variables that failed the Shapiro-Wilk or the Levene test were analyzed with non-parametric statistics using the one-way Kruskal-Wallis analysis of variance on ranks followed by Nemenyi test post hoc and Mann-Whitney rank sum tests for pairwise multiple comparisons. Variables that passed the normality test were analyzed by means of one-way ANOVA followed by Tukey post hoc test for multiple comparisons or by Student's *t* test for comparing two groups. A *p*-value of <0.05 was used as a cutoff for statistical significance. Results are presented as the means ± SEM. The statistical tests are described in each figure legend.

	MO sequence	Dose	Reference
MObarhl1-1	CCCAAATCCGTTAGACCCTTCCATG	15ng	This study
MObarhl1-2	AAAGCCTTGTTCGACTCTCACAATG	20ng	This study
MOct	CCTCTTACCTCAGTTACAATTTATA	20ng	GeneTools

Table 2: Morpholino (MO) oligonucleotide sequences used in this study

Primary Ab	**Source**	**Host**	**Dilution**	**Use**
Barhl2	Covalab	Rabbit	1:500	Western Blot
HA epitope	Roche High Affinity clone 3F10	Rat	1:1000	Western Blot
c-Myc epitope	Santa Cruz Biotechnology clone 9E10	Mouse	1:5000	Western Blot
Flag epitope	Sigma-Aldrich F7425	Rabbit	1:1000	Western Blot (Extracts from HEK293T)

Flag epitope	Sigma-Aldrich F3165	Mouse	1:1000	Western Blot (Extracts from *Xenopus* embryos)
Actin epitope	Sigma-Aldrich A2066	Rabbit	1:2000	Western Blot

Table 3: Primary antibodies (Ab) used in this study

Secondary Ab	**Source**	**Host**	**Dilution**	**Use**
HRP anti-mouse IgG	Jackson ImmunoResearch 115-035-003	Goat	1:10 000	Western Blot
HRP anti-rabbit IgG	Jackson ImmunoResearch 111-035-003	Goat	1:10 000	Western Blot
HRP anti-rat IgG light chain specific	Jackson ImmunoResearch 112-035-175	Goat	1:10 000	Western Blot

Table 4: Secondary antibodies (Ab) used in this study

REFERENCES

Ables, J. L., Breunig, J. J., Eisch, A. J. and Rakic, P. (2011). Not(ch) just development: Notch signalling in the adult brain. *Nat Rev Neurosci* **12**, 269–283.

Abràmoff, M. D., Magalhães, P. J. and Ram, S. J. (2004). Image processing with ImageJ. *Biophotonics international* **11**, 36–42.

Acar, A., Hidalgo-Sastre, A., Leverentz, M. K., Mills, C. G., Woodcock, S., Baron, M., Collu, G. M. and Brennan, K. (2021). Inhibition of Wnt signalling by Notch via two distinct mechanisms. *Sci Rep* **11**, 9096.

Adachi, T., Miyashita, S., Yamashita, M., Shimoda, M., Okonechnikov, K., Chavez, L., Kool, M., Pfister, S. M., Inoue, T., Kawauchi, D., et al. (2021). Notch Signaling between Cerebellar Granule Cell Progenitors. *eNeuro* **8**, ENEURO.0468-20.2021.

Aldinger, K. A., Thomson, Z., Phelps, I. G., Haldipur, P., Deng, M., Timms, A. E., Hirano, M., Santpere, G., Roco, C., Rosenberg, A. B., et al. (2021). Spatial and cell type transcriptional landscape of human cerebellar development. *Nature Neuroscience* **24**, 1163–1175.

Alunni, A. and Bally-Cuif, L. (2016). A comparative view of regenerative neurogenesis in vertebrates. *Development* **143**, 741–753.

Andrews, S. (2010). FastQC: a quality control tool for high throughput sequence data.

Arce, L., Yokoyama, N. N. and Waterman, M. L. (2006). Diversity of LEF/TCF action in development and disease. *Oncogene* **25**, 7492–7504.

Aruga, J. (2004). The role of Zic genes in neural development. *Molecular and Cellular Neuroscience* **26**, 205–221.

Aruga, J. and Millen, K. J. (2018). ZIC1 function in normal cerebellar development and human developmental pathology. *Zic family* 249–268.

Bardou, J. An interactive Venn diagram viewer. *BMC Bioinformatics*.

Bayerl, J., Ayyash, M., Shani, T., Manor, Y. S., Gafni, O., Massarwa, R., Kalma, Y., Aguilera-Castrejon, A., Zerbib, M., Amir, H., et al. (2021). Principles of signaling pathway modulation for enhancing human naive pluripotency induction. *Cell Stem Cell* **28**, 1549-1565.e12.

Belmonte-Mateos, C., Meister, L. and Pujades, C. (2023). Hindbrain rhombomere centers harbor a heterogenous population of dividing progenitors which rely on Notch signaling. *Front. Cell Dev. Biol.* **11**, 1268631.

Ben-Arie, N., Bellen, H. J., Armstrong, D. L., McCall, A. E., Gordadze, P. R., Guo, Q., Matzuk, M. M. and Zoghbi, H. Y. (1997). Math1 is essential for genesis of cerebellar granule neurons. *Nature* **390**, 169–172.

Borday, C., Parain, K., Thi Tran, H., Vleminckx, K., Perron, M. and Monsoro-Burq, A. H. (2018). An atlas of Wnt activity during embryogenesis in Xenopus tropicalis. *PLoS ONE* **13**, e0193606.

Bou-Rouphael, J. and Durand, B. C. (2021). T-Cell Factors as Transcriptional Inhibitors: Activities and Regulations in Vertebrate Head Development. *Frontiers in Cell and Developmental Biology* 3263.

Bowman, A. N., Van Amerongen, R., Palmer, T. D. and Nusse, R. (2013). Lineage tracing with Axin2 reveals distinct developmental and adult populations of Wnt/β-catenin–responsive neural stem cells. *Proceedings of the National Academy of Sciences* **110**, 7324–7329.

Bulfone, A. (2000). Barhl1, a gene belonging to a new subfamily of mammalian homeobox genes, is expressed in migrating neurons of the CNS. *Human Molecular Genetics* **9**, 1443–1452.

Butts, T., Hanzel, M. and Wingate, R. J. (2014). Transit amplification in the amniote cerebellum evolved via a heterochronic shift in NeuroD1 expression. *Development* **141**, 2791–2795.

Carta, I., Chen, C. H., Schott, A. L., Dorizan, S. and Khodakhah, K. (2019). Cerebellar modulation of the reward circuitry and social behavior. *Science* **363**, eaav0581.

Carter, R. A., Bihannic, L., Rosencrance, C., Hadley, J. L., Tong, Y., Phoenix, T. N., Natarajan, S., Easton, J., Northcott, P. A. and Gawad, C. (2018). A Single-Cell Transcriptional Atlas of the Developing Murine Cerebellum. *Current Biology* **28**, 2910-2920.e2.

Chellappa, R., Li, S., Pauley, S., Jahan, I., Jin, K. and Xiang, M. (2008). Barhl1 Regulatory Sequences Required for Cell-Specific Gene Expression and Autoregulation in the Inner Ear and Central Nervous System. *Mol Cell Biol* **28**, 1905–1914.

Cinnamon, E., Helman, A., Ben-Haroush Schyr, R., Orian, A., Jiménez, G. and Paroush, Z. (2008). Multiple RTK pathways downregulate Groucho-mediated repression in *Drosophila* embryogenesis. *Development* **135**, 829–837.

D'Amico, L. A., Boujard, D. and Coumailleau, P. (2013). The Neurogenic Factor NeuroD1 Is Expressed in Post-Mitotic Cells during Juvenile and Adult Xenopus Neurogenesis and Not in Progenitor or Radial Glial Cells. *PLOS ONE* **8**, e66487.

Daniels, D. L. and Weis, W. I. (2005). β-catenin directly displaces Groucho/TLE repressors from Tcf/Lef in Wnt-mediated transcription activation. *Nat Struct Mol Biol* **12**, 364–371.

Deverett, B., Koay, S. A., Oostland, M. and Wang, S. S. (2018). Cerebellar involvement in an evidence-accumulation decision-making task. *elife* **7**,.

Ding, Q., Chen, H., Xie, X., Libby, R. T., Tian, N. and Gan, L. (2009). BARHL2 Differentially Regulates the Development of Retinal Amacrine and Ganglion Neurons. *Journal of Neuroscience* **29**, 3992–4003.

Ding, W. Y., Huang, J. and Wang, H. (2020). Waking up quiescent neural stem cells: Molecular mechanisms and implications in neurodevelopmental disorders. *PLoS genetics* **16**, e1008653.

Dobin, A., Davis, C. A., Schlesinger, F., Drenkow, J., Zaleski, C., Jha, S., Batut, P., Chaisson, M. and Gingeras, T. R. (2013). STAR: ultrafast universal RNA-seq aligner. *Bioinformatics* **29**, 15–21.

Eiraku, M., Tohgo, A., Ono, K., Kaneko, M., Fujishima, K., Hirano, T. and Kengaku, M. (2005). DNER acts as a neuron-specific Notch ligand during Bergmann glial development. *Nature neuroscience* **8**, 873–880.

El Nagar, S., Chakroun, A., Le Greneur, C., Figarella-Branger, D., Di Meglio, T., Lamonerie, T. and Billon, N. (2018). Otx2 promotes granule cell precursor proliferation and Shh-dependent medulloblastoma maintenance in vivo. *Oncogenesis* **7**, 60.

El Yakoubi, W., Borday, C., Hamdache, J., Parain, K., Tran, H. T., Vleminckx, K., Perron, M. and Locker, M. (2012). Hes4 controls proliferative properties of neural stem cells during retinal ontogenesis. *Stem Cells* **30**, 2784–2795.

Espinosa-Sánchez, A., Suárez-Martínez, E., Sánchez-Díaz, L. and Carnero, A. (2020). Therapeutic Targeting of Signaling Pathways Related to Cancer Stemness. *Front. Oncol.* **10**, 1533.

Ewels, P., Magnusson, M., Lundin, S. and Käller, M. (2016). MultiQC: summarize analysis results for multiple tools and samples in a single report. *Bioinformatics* **32**, 3047–3048.

Fendler, A., Bauer, D., Busch, J., Jung, K., Wulf-Goldenberg, A., Kunz, S., Song, K., Myszczyszyn, A., Elezkurtaj, S., Erguen, B., et al. (2020). Inhibiting WNT and NOTCH in renal cancer stem cells and the implications for human patients. *Nat Commun* **11**, 929.

Flora, A., Klisch, T. J., Schuster, G. and Zoghbi, H. Y. (2009). Deletion of Atoh1 disrupts Sonic Hedgehog signaling in the developing cerebellum and prevents medulloblastoma. *Science* **326**, 1424–1427.

Fortriede, J. D., Pells, T. J., Chu, S., Chaturvedi, P., Wang, D., Fisher, M. E., James-Zorn, C., Wang, Y., Nenni, M. J. and Burns, K. A. (2020). Xenbase: deep integration of GEO & SRA RNA-seq and ChIP-seq data in a model organism database. *Nucleic Acids Research* **48**, D776–D782.

Fossat, N., Chatelain, G., Brun, G. and Lamonerie, T. (2006). Temporal and spatial delineation of mouse Otx2 functions by conditional self-knockout. *EMBO reports* **7**, 824–830.

Garbe, D. S. and Ring, R. H. (2012). Investigating Tonic Wnt Signaling Throughout the Adult CNS and in the Hippocampal Neurogenic Niche of BatGal and Ins-TopGal Mice. *Cell Mol Neurobiol* **32**, 1159–1174.

Giachino, C. and Taylor, V. (2014). Notching up neural stem cell homogeneity in homeostasis and disease. *Front. Neurosci.* **8**,.

Gona, A. G. (1972). Morphogenesis of the cerebellum of the frog tadpole during spontaneous metamorphosis. *Journal of Comparative Neurology* **146**, 133–142.

Grbavec, D., Lo, R., Liu, Y. and Stifani, S. (1998). Transducin-like Enhancer of split 2, a mammalian homologue of Drosophila Groucho, acts as a transcriptional repressor, interacts with Hairy/Enhancer of split proteins, and is expressed during neuronal development. *Eur J Biochem* **258**, 339–349.

Haldipur, P., Millen, K. J. and Aldinger, K. A. (2022). Human Cerebellar Development and Transcriptomics: Implications for Neurodevelopmental Disorders. *Annu. Rev. Neurosci.* **45**, 515–531.

Hanzel, M., Rook, V. and Wingate, R. J. (2019). Mitotic granule cell precursors undergo highly dynamic morphological transitions throughout the external germinal layer of the chick cerebellum. *Scientific reports* **9**, 1–13.

Hendrikse, L. D., Haldipur, P., Saulnier, O., Millman, J., Sjoboen, A. H., Erickson, A. W., Ong, W., Gordon, V., Coudière-Morrison, L., Mercier, A. L., et al. (2022). Failure of human rhombic lip differentiation underlies medulloblastoma formation. *Nature* **609**, 1021–1028.

Herrick, C. J. (1914). The cerebellum of Necturus and other urodele Amphibia. *Journal of Comparative Neurology* **24**, 1–29.

Hibi, M., Matsuda, K., Takeuchi, M., Shimizu, T. and Murakami, Y. (2017). Evolutionary mechanisms that generate morphology and neural-circuit diversity of the cerebellum. *Development, growth & differentiation* **59**, 228–243.

Hikasa, H., Ezan, J., Itoh, K., Li, X., Klymkowsky, M. W. and Sokol, S. Y. (2010). Regulation of TCF3 by Wnt-Dependent Phosphorylation during Vertebrate Axis Specification. *Developmental Cell* **19**, 521–532.

Hoppler, S. and Waterman, M. L. (2014). Evolutionary diversification of vertebrate TCF/LEF structure, function, and regulation. *Wnt signaling in development and disease: Molecular mechanisms and biological functions* 225–237.

Hoshino, M., Nakamura, S., Mori, K., Kawauchi, T., Terao, M., Nishimura, Y. V., Fukuda, A., Fuse, T., Matsuo, N. and Sone, M. (2005). Ptf1a, a bHLH transcriptional gene, defines GABAergic neuronal fates in cerebellum. *Neuron* **47**, 201–213.

Houtmeyers, R., Souopgui, J., Tejpar, S. and Arkell, R. (2013). The ZIC gene family encodes multi-functional proteins essential for patterning and morphogenesis. *Cellular and Molecular Life Sciences* **70**, 3791–3811.

Hsieh, F.-Y., Ma, T.-L., Shih, H.-Y., Lin, S.-J., Huang, C.-W., Wang, H.-Y. and Cheng, Y.-C. (2013). Dner inhibits neural progenitor proliferation and induces neuronal and glial differentiation in zebrafish. *Developmental biology* **375**, 1–12.

Imayoshi, I., Sakamoto, M., Yamaguchi, M., Mori, K. and Kageyama, R. (2010). Essential roles of Notch signaling in maintenance of neural stem cells in developing and adult brains. *Journal of Neuroscience* **30**, 3489–3498.

Inoue, T., Ota, M., Ogawa, M., Mikoshiba, K. and Aruga, J. (2007). Zic1 and Zic3 regulate medial forebrain development through expansion of neuronal progenitors. *Journal of Neuroscience* **27**, 5461–5473.

Islam, M. M. and Zhang, C.-L. (2015). TLX: A master regulator for neural stem cell maintenance and neurogenesis. *Biochimica et Biophysica Acta (BBA)-Gene Regulatory Mechanisms* **1849**, 210–216.

Jacobs, C. T. and Huang, P. (2019). Notch signalling maintains Hedgehog responsiveness via a Gli-dependent mechanism during spinal cord patterning in zebrafish. *eLife* **8**, e49252.

Joyner, A. and Bayin, N. S. (2022). Cerebellum lineage allocation, morphogenesis and repair: impact of interplay amongst cells. *Development (2022) 149 (18): dev185587.*

Juraver-Geslin, H. A., Ausseil, J. J., Wassef, M. and Durand, B. C. (2011). Barhl2 limits growth of the diencephalic primordium through Caspase3 inhibition of -catenin activation. *Proceedings of the National Academy of Sciences* **108**, 2288–2293.

Juraver-Geslin, H. A., Gómez-Skarmeta, J. L. and Durand, B. C. (2014). The conserved barH-like homeobox-2 gene barhl2 acts downstream of orthodentricle-2 and together with iroquois-3 in establishment of the caudal forebrain signaling center induced by Sonic Hedgehog. *Developmental Biology* **396**, 107–120.

Kageyama, R., Shimojo, H. and Ohtsuka, T. (2019). Dynamic control of neural stem cells by bHLH factors. *Neuroscience Research* **138**, 12–18.

Kandel, P., Semerci, F., Mishra, R., Choi, W., Bajic, A., Baluya, D., Ma, L., Chen, K., Cao, A. C., Phongmekhin, T., et al. (2022). Oleic acid is an endogenous ligand of TLX/NR2E1 that triggers hippocampal neurogenesis. *Proc. Natl. Acad. Sci. U.S.A.* **119**, e2023784119.

Kawauchi, D. and Saito, T. (2008). Transcriptional cascade from Math1 to Mbh1 and Mbh2 is required for cerebellar granule cell differentiation. *Developmental Biology* **322**, 345–354.

Khouri-Farah, N., Guo, Q., Morgan, K., Shin, J. and Li, J. Y. H. (2022). Integrated single-cell transcriptomic and epigenetic study of cell state transition and lineage commitment in embryonic mouse cerebellum. *Sci. Adv.* **8**, eabl9156.

Kim, D., Langmead, B. and Salzberg, S. L. (2015). HISAT: a fast spliced aligner with low memory requirements. *Nature methods* **12**, 357–360.

Kjolby, R. A., Truchado-Garcia, M., Iruvanti, S. and Harland, R. M. (2019). Integration of Wnt and FGF signaling in the Xenopus gastrula at TCF and Ets binding sites shows the importance of short-range repression by TCF in patterning the marginal zone. *Development* **146**, dev179580.

Klisch, T. J., Xi, Y., Flora, A., Wang, L., Li, W. and Zoghbi, H. Y. (2011). In vivo Atoh1 targetome reveals how a proneural transcription factor regulates cerebellar development. *Proceedings of the National Academy of Sciences* **108**, 3288–3293.

Kobayashi, T. and Kageyama, R. (2014). Expression Dynamics and Functions of Hes Factors in Development and Diseases. In *Current Topics in Developmental Biology*, pp. 263–283. Elsevier.

Konno, D., Iwashita, M., Satoh, Y., Momiyama, A., Abe, T., Kiyonari, H. and Matsuzaki, F. (2012). The mammalian DM domain transcription factor Dmrta2 is required for early embryonic development of the cerebral cortex.

Lackey, E. P., Heck, D. H. and Sillitoe, R. V. (2018). Recent advances in understanding the mechanisms of cerebellar granule cell development and function and their contribution to behavior. *F1000Res* **7**, 1142.

Lampada, A. and Taylor, V. (2023). Notch signaling as a master regulator of adult neurogenesis. *Front. Neurosci.* **17**, 1179011.

Leto, K., Arancillo, M., Becker, E. B. E., Buffo, A., Chiang, C., Ding, B., Dobyns, W. B., Dusart, I., Haldipur, P., Hatten, M. E., et al. (2016). Consensus Paper: Cerebellar Development. *Cerebellum* **15**, 789–828.

Li, S., Qiu, F., Xu, A., Price, S. M. and Xiang, M. (2004). Barhl1 Regulates Migration and Survival of Cerebellar Granule Cells by Controlling Expression of the Neurotrophin-3 Gene. *Journal of Neuroscience* **24**, 3104–3114.

Liao, Y., Smyth, G. K. and Shi, W. (2014). featureCounts: an efficient general purpose program for assigning sequence reads to genomic features. *Bioinformatics* **30**, 923–930.

Lim, L. S., Loh, Y.-H., Zhang, W., Li, Y., Chen, X., Wang, Y., Bakre, M., Ng, H.-H. and Stanton, L. W. (2007). Zic3 is required for maintenance of pluripotency in embryonic stem cells. *Molecular biology of the cell* **18**, 1348–1358.

Lim, L. S., Hong, F. H., Kunarso, G. and Stanton, L. W. (2010). The pluripotency regulator Zic3 is a direct activator of the Nanog promoter in ESCs. *Stem cells* **28**, 1961–1969.

Lin, C. Y., Erkek, S., Tong, Y., Yin, L., Federation, A. J., Zapatka, M., Haldipur, P., Kawauchi, D., Risch, T., Warnatz, H.-J., et al. (2016). Active medulloblastoma enhancers reveal subgroup-specific cellular origins. *Nature* **530**, 57–62.

Liu, F., van den Broek, O., Destrée, O. and Hoppler, S. (2005). Distinct roles for *Xenopus* Tcf/Lef genes in mediating specific responses to Wnt/β-catenin signalling in mesoderm development. *Development* **132**, 5375–5385.

Love, M. I., Huber, W. and Anders, S. (2014). Moderated estimation of fold change and dispersion for RNA-seq data with DESeq2. *Genome biology* **15**, 1–21.

Ma, N., Puls, B. and Chen, G. (2022). Transcriptomic analyses of NeuroD1-mediated astrocyte-to-neuron conversion. *Developmental Neurobiology* **82**, 375–391.

Machold, R. and Fishell, G. (2005). Math1 is expressed in temporally discrete pools of cerebellar rhombic-lip neural progenitors. *Neuron* **48**, 17–24.

Machold, R. P., Kittell, D. J. and Fishell, G. J. (2007). Antagonism between Notch and bone morphogenetic protein receptor signaling regulates neurogenesis in the cerebellar rhombic lip. *Neural Dev* **2**, 5.

Mashal, R. D., Koontz, J. and Sklar, J. (1995). Detection of mutations by cleavage of DNA heteroduplexes with bacteriophage resolvases. *Nature genetics* **9**, 177–183.

Miyashita, S. and Hoshino, M. (2022). Transit Amplifying Progenitors in the Cerebellum: Similarities to and Differences from Transit Amplifying Cells in Other Brain Regions and between Species. *Cells* **11**, 726.

Miyata, T., Maeda, T. and Lee, J. E. (1999). NeuroD is required for differentiation of the granule cells in the cerebellum and hippocampus. *Genes & development* **13**, 1647–1652.

Mo, Z., Li, S., Yang, X. and Xiang, M. (2004). Role of the *Barhl2* homeobox gene in the specification of glycinergic amacrine cells. *Development* **131**, 1607–1618.

Molenaar, M., van de Wetering, M., Oosterwegel, M., Peterson-Maduro, J., Godsave, S., Korinek, V., Roose, J., Destrée, O. and Clevers, H. (1996). XTcf-3 Transcription

Factor Mediates β-Catenin-Induced Axis Formation in Xenopus Embryos. *Cell* **86**, 391–399.

Myers, C. T., Appleby, S. C. and Krieg, P. A. (2014). Use of small molecule inhibitors of the Wnt and Notch signaling pathways during Xenopus development. *Methods* **66**, 380–389.

Nakamura, Y., de Paiva Alves, E., Veenstra, G. J. and Hoppler, S. (2016). Tissue- and stage-specific Wnt target gene expression is controlled subsequent to β-catenin recruitment. *Development* dev.131664.

Nieuwkoop, P. and Faber, J. (1994). Normal table of Xenopus laevis (Daudin) garland publishing. *New York* **252**,.

Nusse, R. (2008). Wnt signaling and stem cell control. *Cell research* **18**, 523–527.

Pascual, M., Abasolo, I., Mingorance-Le Meur, A., Martínez, A., Del Rio, J. A., Wright, C. V., Real, F. X. and Soriano, E. (2007). Cerebellar GABAergic progenitors adopt an external granule cell-like phenotype in the absence of Ptf1a transcription factor expression. *Proceedings of the National Academy of Sciences* **104**, 5193–5198.

Ramirez, M., Badayeva, Y., Yeung, J., Wu, J., Yang, E., Trost, B., Scherer, S. W., Goldowitz, D., and FANTOM 5 Consortium (2021). Temporal analysis of enhancers during mouse brain development reveals dynamic regulatory function and identifies novel regulators of cerebellar development. *bioRxiv*.

Reeber, S. L., Otis, T. S. and Sillitoe, R. V. (2013). New roles for the cerebellum in health and disease. *Front. Syst. Neurosci.* **7**,.

Reig, G., Cabrejos, M. E. and Concha, M. L. (2007). Functions of BarH transcription factors during embryonic development. *Developmental Biology* **302**, 367–375.

Roël, G., Hamilton, F. S., Gent, Y., Bain, A. A., Destrée, O. and Hoppler, S. (2002). Lef-1 and Tcf-3 Transcription Factors Mediate Tissue-Specific Wnt Signaling during Xenopus Development. *Current Biology* **12**, 1941–1945.

Roelink, H. and Nusse, R. (1991). Expression of two members of the Wnt family during mouse development--restricted temporal and spatial patterns in the developing neural tube. *Genes Dev.* **5**, 381–388.

Roose, J., Molenaar, M., Peterson, J., Hurenkamp, J., Brantjes, H., Moerer, P., Van De Wetering, M., Destrée, O. and Clevers, H. (1998). The Xenopus Wnt effector XTcf-3 interacts with Groucho-related transcriptional repressors. *Nature* **395**, 608–612.

Schneider, C. A., Rasband, W. S. and Eliceiri, K. W. (2012). NIH Image to ImageJ: 25 years of image analysis. *Nature Methods* **9**, 671–675.

Schwartz, H. T. and Horvitz, H. R. (2007). The C. elegans protein CEH-30 protects male-specific neurons from apoptosis independently of the Bcl-2 homolog CED-9. *Genes & Development* **21**, 3181–3194.

Selvadurai, H. J. and Mason, J. O. (2011). Wnt/β-catenin Signalling Is Active in a Highly Dynamic Pattern during Development of the Mouse Cerebellum. *PLoS ONE* **6**, e23012.

Sena, E., Rocques, N., Borday, C., Amin, H. S. M., Parain, K., Sitbon, D., Chesneau, A. and Durand, B. C. (2019). Barhl2 maintains T-cell factors as repressors, and thereby

switches off the Wnt/β-Catenin response driving Spemann organizer formation. *Development* dev.173112.

Shi, F., Cheng, Y., Wang, X. L. and Edge, A. S. (2010). β-catenin up-regulates Atoh1 expression in neural progenitor cells by interaction with an Atoh1 3′ enhancer. *Journal of Biological Chemistry* **285**, 392–400.

Shy, B. R., Wu, C.-I., Khramtsova, G. F., Zhang, J. Y., Olopade, O. I., Goss, K. H. and Merrill, B. J. (2013). Regulation of Tcf7l1 DNA Binding and Protein Stability as Principal Mechanisms of Wnt/β-Catenin Signaling. *Cell Reports* **4**, 1–9.

Smith, K. S., Bihannic, L., Gudenas, B. L., Haldipur, P., Tao, R., Gao, Q., Li, Y., Aldinger, K. A., Iskusnykh, I. Y., Chizhikov, V. V., et al. (2022). Unified rhombic lip origins of group 3 and group 4 medulloblastoma. *Nature* **609**, 1012–1020.

Sokol, S. Y. (2011). Maintaining embryonic stem cell pluripotency with Wnt signaling. *Development* **138**, 4341–4350.

Solecki, D. J., Liu, X. L., Tomoda, T., Fang, Y. and Hatten, M. E. (2001). Activated Notch2 signaling inhibits differentiation of cerebellar granule neuron precursors by maintaining proliferation. *Neuron* **31**, 557–568.

Tran, H. T. and Vleminckx, K. (2014). Design and use of transgenic reporter strains for detecting activity of signaling pathways in Xenopus. *Methods* **66**, 422–432.

Tran, H. T., Sekkali, B., Van Imschoot, G., Janssens, S. and Vleminckx, K. (2010). Wnt/β-catenin signaling is involved in the induction and maintenance of primitive hematopoiesis in the vertebrate embryo. *Proceedings of the National Academy of Sciences* **107**, 16160–16165.

Urbán, N., Blomfield, I. M. and Guillemot, F. (2019). Quiescence of adult mammalian neural stem cells: a highly regulated rest. *Neuron* **104**, 834–848.

Wang, V. Y., Rose, M. F. and Zoghbi, H. Y. (2005). Math1 expression redefines the rhombic lip derivatives and reveals novel lineages within the brainstem and cerebellum. *Neuron* **48**, 31–43.

Wang, Y., Liu, H.-K. and Schütz, G. (2013). Role of the nuclear receptor Tailless in adult neural stem cells. *Mechanisms of Development* **130**, 388–390.

Wizeman, J. W., Guo, Q., Wilion, E. M. and Li, J. Y. (2019). Specification of diverse cell types during early neurogenesis of the mouse cerebellum. *eLife* **8**, e42388.

Wu, C.-I., Hoffman, J. A., Shy, B. R., Ford, E. M., Fuchs, E., Nguyen, H. and Merrill, B. J. (2012). Function of Wnt/β-catenin in counteracting Tcf3 repression through the Tcf3–β-catenin interaction. *Development* **139**, 2118–2129.

Wu, T., Hu, E., Xu, S., Chen, M., Guo, P., Dai, Z., Feng, T., Zhou, L., Tang, W., Zhan, L., et al. (2021). clusterProfiler 4.0: A universal enrichment tool for interpreting omics data. *The Innovation* **2**, 100141.

Yamada, M., Seto, Y., Taya, S., Owa, T., Inoue, Y. U., Inoue, T., Kawaguchi, Y., Nabeshima, Y. and Hoshino, M. (2014). Specification of spatial identities of cerebellar neuron progenitors by ptf1a and atoh1 for proper production of GABAergic and glutamatergic neurons. *Journal of Neuroscience* **34**, 4786–4800.

Yao, Y., Minor, P. J., Zhao, Y.-T., Jeong, Y., Pani, A. M., King, A. N., Symmons, O., Gan, L., Cardoso, W. V., Spitz, F., et al. (2016). Cis-regulatory architecture of a brain signaling center predates the origin of chordates. *Nat Genet* **48**, 575–580.

Yeung, J. and Goldowitz, D. (2017). Wls expression in the rhombic lip orchestrates the embryonic development of the mouse cerebellum. *Neuroscience* **354**, 30–42.

Yeung, J., Ha, T. J., Swanson, D. J., Choi, K., Tong, Y. and Goldowitz, D. (2014). Wls Provides a New Compartmental View of the Rhombic Lip in Mouse Cerebellar Development. *J. Neurosci.* **34**, 12527.

Young, F. I., Keruzore, M., Nan, X., Gennet, N., Bellefroid, E. J. and Li, M. (2017). The doublesex-related Dmrta2 safeguards neural progenitor maintenance involving transcriptional regulation of Hes1. *Proc. Natl. Acad. Sci. U.S.A.* **114**,.

Zhang, T., Liu, T., Mora, N., Guegan, J., Bertrand, M., Contreras, X., Hansen, A. H., Streicher, C., Anderle, M., Danda, N., et al. (2021). Generation of excitatory and inhibitory neurons from common progenitors via Notch signaling in the cerebellum. *Cell Reports* **35**, 109208.

FIGURES LEGENDS

Figure 1: Temporal and spatial expression pattern of genes involved in granule neuron progenitors' (GNP) development

(A) Neural tube dissection and analysis. (a) representation of stage (st.) 45 *X. laevis* embryo. Following ISH, neural tubes are dissected as shown on the middle (entire neural tube) and (b) (a focus on the rhombomere 1 (R1)) panels. The proliferation marker *nmyc* is expressed in the upper rhombic lip (URL) (blue arrow), the ventricular zone VZ (white arrow). Red dotted lines delineate rhombomere 1 (R1) located caudal to the midbrain-hindbrain boundary (MHB). *nmyc* marks proliferating progenitors at the boundary between R1 and R2 and is used as a marker of cerebellar primordium's caudal limit. The cerebellar plate (CP) is indicated (green arrow). (c) Scheme of a st. 42 Xenopus half R1. (B) ISH analysis of GNP markers in *X. laevis* embryos at the indicated Nieuwkoop and Faber stages. Shown are dorsal and lateral views of the R1. From st. 41 to st. 48 stem/progenitor markers *atoh1 (Ba-b'), nmyc* (Ca-b'), *hes5.1* (Da, a') and *hes4* (Db, b') display a strong expression in the URL and in the EGL. At st. 41 committed GNP markers *pax6* (Ea, a') and *barhl1* (Fa, a'), together with the differentiation marker *neurod1* (Ga, a') are detected in the caudal EGL and the CP. (Ha, a') *otx2* expression is first detected in caudal EGL and within the CP at st. 48 (Hb, b'). As development proceeds, transcripts for these markers are detected in the CP and their expression significantly increases in this area (E-G, b, b'). Fully differentiated GNs settling in the internal granule layer (IGL) are stained with *neurod1* as observed in lateral views of st. 48 *X. laevis* embryos. The CP is devoid of *atoh1, hes5.1, hes4,* and *nmyc* expressions. CP: cerebellar plate; VZ: ventricular zone; URL: upper rhombic lip; EGL: external granule layer; R: rhombomere; MHB: midbrain-hindbrain boundary. Scale bar 150µm.

Figure 2: Tcf activity is required for the induction of the URL and its inhibition by Barhl1 is necessary for the proper progression of GNPs development

(A) Overexpression of *tcf7l1-Δβcat-GR* inhibits/abolishes *atoh1* expression in a dose dependent manner. ISH analysis of *atoh1* expression in the rhombomere 1 (R1) showing dorsal views (a, b) and lateral views of control sides (a', b') and injected sides (a", b") of stage 45 *X. laevis* embryos unilaterally injected with 200pg (a, a', a")(n= or 100pg (b, b', b") of *tcf7l1-Δβcat-GR.* The non-injected side is an internal control. **(B) Forced expression of *tcf7l1-Δβcat-GR at low doses* stimulates GNP differentiation.** ISH analysis of the commitment/differentiation markers *barhl1, pax6* and *neurod1* (a-c) in stage 45 *X. laevis* embryos unilaterally injected with 100pg of *tcf7l1-Δβcat-GR.* **(C) *barhl1* overexpression phenocopies defects of *tcf7l1dn* overexpression.** Dorsal views showing *atoh1, barhl1* and *neurod1* (a, b, and c respectively) expressions in the R1 primordium of stage 45 *X. laevis* embryos injected with *mBarhl1GR* (200pg). Lateral views of *atoh1* expression in control side (a') and injected side (a") are shown. Integrated densities *(IntDen)* of markers' expressions were measured. Ratio of markers expression in injected side over control side is represented (Ac; Bd; Cd). Data are presented as means ± SEM. Each tadpole is represented by a square. Dotted lines separate injected and control sides. Scale bar 150µm. Square brackets delineate R1. Dex: dexamethasone; *inj*: injected side. Statistical analysis C: One-way ANOVA ($F_{(2,31)}$=437.5; $p < 0.001$) followed by post hoc Tukey test. Bd, Cd: student's t-test. ** $p \leq 0.01$; *** $p \leq 0.001$; **** $p \leq 0.0001$.

Figure 3: In the cerebellar URL, antagonistic activities of Barhl1 and Tcf are required for proper development of GNPs

(A-D) **Morpholino (MO)-mediated inhibition of Barhl1 induces an ectopic expansion of *atoh1* in the upper rhombic lip (URL) and cerebellar plate and delays GNPs differentiation.** *ISH* of st. 45 *X. laevis* embryos unilaterally injected with (A) *MObarhl1-1* (15ng) and (B) *MObarhl1-2* (20ng). The non-injected side is an internal control. Shown are dorsal views of *atoh1* (Aa; Ba), *pax6* (Ab; Bb), and *neurod1* (Da; Db) in the cerebellar anlage. Lateral views of *atoh1* expression in control (Aa', Ba') and injected sides (Aa", Ba"). (C) Quantification of (A) and (B). (Da-c) *MObarhl1* phenotype is rescued by *mBarhl1* overexpression. ISH of *neurod1* expression in embryos co-injected with *MObarhl1-1* and *mBarhl1* mRNA. (Dd) Quantification of (D). **(E) Inhibition of Tcf activity compensates for Barhl1 depletion.** ISH analysis of *pax6* expression in the cerebellar anlage in st. 48 *X. laevis* embryos unilaterally injected with (Ea) *MObarhl1-1* (15ng), (Eb) *tcf7l1-Δβcat-GR* at 100pg and (Ec) *tcf7l1-Δβcat-GR* at 200pg. *pax6* expression was rescued when *MObarhl1-1* (15ng) was co-injected with *tcf7l1-Δβcat-GR* at 100pg (Ed) and at 200pg (Ee). **(C, Dd, Ef) Quantification**: Ratio of markers expression in injected side over control side is indicated as mean ± s.e.m. Each tadpole is represented by a square. Dotted lines separate injected and control sides. Scale bar 150µm. *inj*: injected side. Statistical analysis (C) *atoh1*: One-way ANOVA($F_{(2,21)}$=19.9; $p < 0.001$) followed by post hoc Tukey test. *pax6*: One-way ANOVA ($F_{(2,14)}$=8.63; $p = 0.004$) followed by post hoc Tukey test. (Dd): Kruskal-Wallis test (Chi square=35.6 *p<0.001*, df=3) followed by Nemenyi test post hoc. (Ef): One-way ANOVA($F_{(4,31)}$=32.9; $p < 0.001$) followed by post hoc Tukey test. Data are presented as means ± SEM* $p \leq 0.05$; ** $p \leq 0.01$; *** $p \leq 0.001$; **** $p \leq 0.0001$.

Figure 4: Barhl1 physically interacts with Tcf7l1 and Gro and limits Tcf transcriptional activity (A) HEK293T cells were transfected with plasmids encoding indicated tagged proteins. Cell lysates were immunoprecipitated (IP) by anti-cMyc antibody. Input and IP samples were subjected to western blot analysis using indicated antibodies. Equal amounts of protein lysates were loaded on SDS-gel. (Aa) Barhl1 interacts with Groucho 4 (Gro4) and Tcf7l1. (Ab) The interaction between Barhl1 and Tcf7l1 is detected in the presence and in the absence of Gro. (Ac) Barhl1 interacts with Tcf7l1, Tcf7l2 and Tcf7. (B) Tcf activity is detected in the URL in an area overlapping with that of *atoh1*, and complementary to that of *barhl1*. ISH in *X. tropicalis* pbin7LefdGFP line at indicated stages *(st.)* showing *gfp* (Tcf activity) (Ba, b, c, d), *atoh1* (Ba', b', c', d') and *barhl1* (Bc", d") expression patterns. (Bc"') DISH showing expression of *barhl1* (blue) and *gfp* (red). Dorsal views of one side of the embryos are shown. (C, D) Barhl1 limits Tcf transcriptional activity *in vivo*. ISH analysis of *gfp* expression in *X. tropicalis* pbin7LefdGFP embryos injected either unilaterally with (Ca) *mBarhl1GR* (200pg) and (Cb) *MObarhl1-1* or before division with (Db) *Crispr-barhl1*. Embryos injected with *Crispr-barhl1* were compared to their wild-type *(WT)* siblings. (E) Interaction between Barhl1 and Gro is required for Barhl1 function. *mBarhl2EHsGR* only contains the two EH1 motifs of Barhl2 and acts as a dominant negative by capturing Gro. (Ea) ISH showing *atoh1* expression in injected versus control side. **(Cc; Dc; Eb) Quantification:** Integrated densities *(IntDen)* of markers' expressions are measured. Ratio of markers expression in injected side over control side is represented and indicated as mean ± s.e.m. Each tadpole is represented by a square. Percentage of phenotype penetrance is quantified in embryos injected with *Crispr/barhl1* versus WT embryos based on indicated criteria. Dotted lines separate injected and control sides. Scale bar 150µm. *inj*: injected side. Statistical analysis (Cc): One-way ANOVA($F_{(2,35)}$=111,3; $p < 0.001$) followed by post hoc Tukey test was carried out. (Dc and Eb): student's t-test two-tailed. Data are presented as means ± SEM * $p \leq 0.05$; *** $p \leq 0.001$; **** $p \leq 0.0001$.

Figure 5: In the URL, Barhl1 activity as an inhibitor of Tcf transcription is required for GNPs to exit their germinative zone and become post-mitotic. (A) Barhl1-KD induces an increase in the URL length associated with increased proliferation within this compartment. (a-d) Imaging of cerebellar anlage of st. 48 *X. laevis* tadpoles unilaterally injected with *MOct* and *MObarhl1-1* (15 ng). Collected neural tubes were stained for the mitotic marker PhosphoHistone-H3 (PHH3) (green) merged with bisbenzimide (BB) (red). In *Xenopus*, the EGL is devoid of proliferating cells. (e-g) Quantifications of (A). The ratio of (e) measured URL length and (f) PHH3+ cells in injected side over control side are represented. Each tadpole is represented by a square. (Ac, d) PHH3 positive cells are ectopically detected in the cerebellar plate (Ac, d white arrow heads) of injected embryos. (g) Percentage of PHH3+ cells located inside the URL compared to those located outside the URL were quantified on the injected side and on the control side. (E) The Barhl1-KD induced increase in URL length is rescued upon co-inhibiting Tcf activity. ISH analysis of *n-myc* expression in the cerebellar anlage of stage 48 *X. laevis* embryos unilaterally injected with (Ba) *MObarhl1-1* (15ng), (Bb) *tcf7l1-Δβcat-GR* at 100pg and (Bc) *tcf7l1-Δβcat-GR* at 200pg. *n-myc* marks the boundaries between different rhombomeres which allows the exact measurement of URL length. URL length was rescued when *MObarhl1-1* (15ng) was co-injected with *tcf7l1-Δβcat-GR* at 100pg (Bd) or at 200pg (Be). Ratio of URL length in injected side over control side is represented (Bf). Data are presented as means ± SEM. Each tadpole is represented by a square. Dotted lines separate injected and control sides. Scale bar 150µm. *inj*: injected side; cp: choroid plexus; URL: Upper Rhombic Lip; VZ: Ventricular Zone; R1-R2: Rhombomere 1 and 2; MHB: Midbrain-Hindbrain Boundary. Statistical analysis Ae, Af: was carried out using student's t-test two-tailed. Bf: One-way ANOVA($F_{(4,49)}$=65.1; $p < 0.001$) followed by post hoc Tukey test. ** $p \leq 0.01$; *** $p \leq 0.001$; **** $p \leq 0.0001$.

Figure 6: RNA-sequencing data processing and analysis

(A) Differentially expressed genes (DEGs) visualization Heatmap displaying expression profiles of most significantly upregulated and downregulated DEGs for each condition (*MObarhl1-1 vs MOct* and *MObarhl1-2 vs MOct*). Each row represents a gene, and each column represents a sample. Results are shown as a gradient from blue (downregulated) to dark orange (upregulated). Heatmap is generated using R package. **(B) Volcano plots** showing a selection of significant DEGs with pAdj < 0.001 in (a) *MObarhl1-1 vs MOct* and (b) *MObarhl1-2 vs MOct*. Upregulated genes with Log2FC>0.4, and downregulated genes with Log2FC<-0.4 are shown. Red and blue dots indicate significant DEGs that are upregulated and downregulated, respectively. Grey dots denote RNAs with non-significant difference. PCA and volcano plots were generated using Galaxy. **(C, D) Gene ontology enrichment comparison.** Shown on Y axis are (C) the altered molecular functions and (D) biological processes for selected (C) upregulated (Log2FC≥0.5, PAdj<0.001), and (D) downregulated (Log2FC≤-0.5, PAdj<0.001) DEGs respectively. Enrichment analysis comparing functional profiles among *MObarhl1-1* and *MObarhl1-2* was performed on the DEGs in common between both conditions. Results are visualized as a dot plot based on indicated gene counts and adjusted p-values for enrichment. Dot size corresponds to the count of differentially expressed genes associated with the molecular function or the biological pathway, and dot color refers to the adjusted P-value for enrichment. **(E) Barhl1 and (F) TCF Cis Regulatory Motifs (CRM) in regulatory regions of MOBarhl1 DEGs**: pie chart of % of *MObarhl1* DEGs located 5Kb or 30Kb upstream or downstream of their TSS as indicated**. (G) ISH analysis of 3 DEGs**: Dorsal views R1 territory of st. 42 *X. laevis* embryos unilaterally injected with

MObarhl1-1 using *hes5.1* as ISH probe *(a) hes5.1, (b) hes5.1 with DMSO, (c) hes5.1 with LY411575*, (d) quantification, (e) Total and average size of the *hes5.1* expression area in embryos grown in LY411757 relative to embryos grown in DMSO. Each tadpole is represented by a square. *inj:* injected side. Statistical analysis was carried out using student's t-test two-tailed. ** $p \leq 0.01$; *** $p \leq 0.001$; **** $p \leq 0.0001$.

Table 1. List of differentially expressed genes identified by RNAseq analysis

The table shows the list of all DEG obtained from the RNAseq experiment for (A) *MObarhl1-1*, (B) *MObarhl1-2* conditions, each compared to *MOcontrol (MOct)*. (C) Gene counts are obtained using FeatureCounts. Genes with adjusted p-value (pAdj) inferior to 0.001 were selected as significant DE genes (DEG). DEG in common between both conditions are also represented.

FIGURES LEGENDS

Figure 1: Temporal and spatial expression pattern of genes involved in granule neuron progenitors' (GNP) development

(A) Neural tube dissection and analysis. (a) representation of stage (st.) 45 *X. laevis* embryo. Following ISH, neural tubes are dissected as shown on the middle (entire neural tube) and (b) (a focus on the rhombomere 1 (R1)) panels. The proliferation marker *nmyc* is expressed in the upper rhombic lip (URL) (blue arrow), the ventricular zone VZ (white arrow). Red dotted lines delineate rhombomere 1 (R1) located caudal to the midbrain-hindbrain boundary (MHB). *nmyc* marks proliferating progenitors at the boundary between R1 and R2 and is used as a marker of cerebellar primordium's caudal limit. The cerebellar plate (CP) is indicated (green arrow). (c) Scheme of a st. 42 Xenopus half R1. (B) ISH analysis of GNP markers in *X. laevis* embryos at the indicated Nieuwkoop and Faber stages. Shown are dorsal and lateral views of the R1. From st. 41 to st. 48 stem/progenitor markers *atoh1 (Ba-b'), nmyc* (Ca-b'), *hes5.1* (Da, a') and *hes4* (Db, b') display a strong expression in the URL and in the EGL. At st. 41 committed GNP markers *pax6* (Ea, a') and *barhl1* (Fa, a'), together with the differentiation marker *neurod1* (Ga, a') are detected in the caudal EGL and the CP. (Ha, a') *otx2* expression is first detected in caudal EGL and within the CP at st. 48 (Hb, b'). As development proceeds, transcripts for these markers are detected in the CP and their expression significantly increases in this area (E-G, b, b'). Fully differentiated GNs settling in the internal granule layer (IGL) are stained with *neurod1* as observed in lateral views of st. 48 *X. laevis* embryos. The CP is devoid of *atoh1, hes5.1, hes4,* and *nmyc* expressions. CP: cerebellar plate; VZ: ventricular zone; URL: upper rhombic lip; EGL: external granule layer; R: rhombomere; MHB: midbrain-hindbrain boundary. Scale bar 150µm.

Figure 2: Tcf activity is required for the induction of the URL and its inhibition by Barhl1 is necessary for the proper progression of GNPs development

(A) Overexpression of *tcf7l1-*Δ*βcat-GR* inhibits/abolishes *atoh1* expression in a dose dependent manner. ISH analysis of *atoh1* expression in the rhombomere 1 (R1) showing dorsal views (a, b) and lateral views of control sides (a', b') and injected sides (a", b") of stage 45 *X. laevis* embryos unilaterally injected with 200pg (a, a', a")(n= or 100pg (b, b', b") of *tcf7l1-*Δ*βcat-GR.* The non-injected side is an internal control. **(B) Forced expression of *tcf7l1-*Δ*βcat-GR at low doses* stimulates GNP differentiation.** ISH analysis of the commitment/differentiation markers *barhl1, pax6* and *neurod1* (a-c) in stage 45 *X. laevis* embryos unilaterally injected with 100pg of *tcf7l1-*Δ*βcat-GR.* **(C) *barhl1* overexpression phenocopies defects of *tcf7l1dn* overexpression.** Dorsal views showing *atoh1, barhl1* and *neurod1* (a, b, and c respectively) expressions in the R1 primordium of stage 45 *X. laevis* embryos injected with *mBarhl1GR* (200pg). Lateral views of *atoh1* expression in control side (a') and injected side (a") are shown. Integrated densities *(IntDen)* of markers' expressions were measured. Ratio of markers expression in injected side over control side is represented (Ac; Bd; Cd). Data are presented as means ± SEM. Each tadpole is represented by a square. Dotted lines separate injected and control sides. Scale bar 150µm. Square brackets delineate R1. Dex: dexamethasone; *inj*: injected side. Statistical analysis C: One-way ANOVA ($F_{(2,31)}$=437.5; $p < 0.001$) followed by post hoc Tukey test. Bd, Cd: student's t-test. ** $p \leq 0.01$; *** $p \leq 0.001$; **** $p \leq 0.0001$.

Figure 3: In the cerebellar URL, antagonistic activities of Barhl1 and Tcf are required for proper development of GNPs

(A-D) **Morpholino (MO)-mediated inhibition of Barhl1 induces an ectopic expansion of *atoh1* in the upper rhombic lip (URL) and cerebellar plate and delays GNPs differentiation.** *ISH* of st. 45 *X. laevis* embryos unilaterally injected with (A) *MObarhl1-1* (15ng) and (B) *MObarhl1-2* (20ng). The non-injected side is an internal control. Shown are dorsal views of *atoh1* (Aa; Ba), *pax6* (Ab; Bb), and *neurod1* (Da; Db) in the cerebellar anlage. Lateral views of *atoh1* expression in control (Aa', Ba') and injected sides (Aa", Ba"). (C) Quantification of (A) and (B). (Da-c) *MObarhl1* phenotype is rescued by *mBarhl1* overexpression. ISH of *neurod1* expression in embryos co-injected with *MObarhl1-1* and *mBarhl1* mRNA. (Dd) Quantification of (D). **(E) Inhibition of Tcf activity compensates for Barhl1 depletion.** ISH analysis of *pax6* expression in the cerebellar anlage in st. 48 *X. laevis* embryos unilaterally injected with (Ea) *MObarhl1-1* (15ng), (Eb) *tcf7l1-Δβcat-GR* at 100pg and (Ec) *tcf7l1-Δβcat-GR* at 200pg. *pax6* expression was rescued when *MObarhl1-1* (15ng) was co-injected with *tcf7l1-Δβcat-GR* at 100pg (Ed) and at 200pg (Ee). **(C, Dd, Ef) Quantification**: Ratio of markers expression in injected side over control side is indicated as mean ± s.e.m. Each tadpole is represented by a square. Dotted lines separate injected and control sides. Scale bar 150µm. *inj*: injected side. Statistical analysis (C) *atoh1*: One-way ANOVA($F_{(2,21)}$=19.9; $p < 0.001$) followed by post hoc Tukey test. *pax6*: One-way ANOVA ($F_{(2,14)}$=8.63; $p = 0.004$) followed by post hoc Tukey test. (Dd): Kruskal-Wallis test (Chi square=35.6 *p<0.001*, df=3) followed by Nemenyi test post hoc. (Ef): One-way ANOVA($F_{(4,31)}$=32.9; $p < 0.001$) followed by post hoc Tukey test. Data are presented as means ± SEM* $p \leq 0.05$; ** $p \leq 0.01$; *** $p \leq 0.001$; **** $p \leq 0.0001$.

Figure 4: Barhl1 physically interacts with Tcf7l1 and Gro and limits Tcf transcriptional activity (A) HEK293T cells were transfected with plasmids encoding indicated tagged proteins. Cell lysates were immunoprecipitated (IP) by anti-cMyc antibody. Input and IP samples were subjected to western blot analysis using indicated antibodies. Equal amounts of protein lysates were loaded on SDS-gel. (Aa) Barhl1 interacts with Groucho 4 (Gro4) and Tcf7l1. (Ab) The interaction between Barhl1 and Tcf7l1 is detected in the presence and in the absence of Gro. (Ac) Barhl1 interacts with Tcf7l1, Tcf7l2 and Tcf7. (B) Tcf activity is detected in the URL in an area overlapping with that of *atoh1*, and complementary to that of *barhl1*. ISH in *X. tropicalis* pbin7LefdGFP line at indicated stages *(st.)* showing *gfp* (Tcf activity) (Ba, b, c, d), *atoh1* (Ba', b', c', d') and *barhl1* (Bc", d") expression patterns. (Bc"') DISH showing expression of *barhl1* (blue) and *gfp* (red). Dorsal views of one side of the embryos are shown. (C, D) Barhl1 limits Tcf transcriptional activity *in vivo*. ISH analysis of *gfp* expression in *X. tropicalis* pbin7LefdGFP embryos injected either unilaterally with (Ca) *mBarhl1GR* (200pg) and (Cb) *MObarhl1-1* or before division with (Db) *Crispr-barhl1*. Embryos injected with *Crispr-barhl1* were compared to their wild-type *(WT)* siblings. (E) Interaction between Barhl1 and Gro is required for Barhl1 function. *mBarhl2EHsGR* only contains the two EH1 motifs of Barhl2 and acts as a dominant negative by capturing Gro. (Ea) ISH showing *atoh1* expression in injected versus control side. **(Cc; Dc; Eb) Quantification:** Integrated densities *(IntDen)* of markers' expressions are measured. Ratio of markers expression in injected side over control side is represented and indicated as mean ± s.e.m. Each tadpole is represented by a square. Percentage of phenotype penetrance is quantified in embryos injected with *Crispr/barhl1* versus WT embryos based on indicated criteria. Dotted lines separate injected and control sides. Scale bar 150µm. *inj*: injected side. Statistical analysis (Cc): One-way ANOVA($F_{(2,35)}$=111,3; $p < 0.001$) followed by

post hoc Tukey test was carried out. (Dc and Eb): student's t-test two-tailed. Data are presented as means ± SEM * $p \leq 0.05$; *** $p \leq 0.001$; **** $p \leq 0.0001$.

Figure 5: In the URL, Barhl1 activity as an inhibitor of Tcf transcription is required for GNPs to exit their germinative zone and become post-mitotic. (A) Barhl1-KD induces an increase in the URL length associated with increased proliferation within this compartment. (a-d) Imaging of cerebellar anlage of st. 48 *X. laevis* tadpoles unilaterally injected with *MOct* and *MObarhl1-1* (15 ng). Collected neural tubes were stained for the mitotic marker PhosphoHistone-H3 (PHH3) (green) merged with bisbenzimide (BB) (red). In *Xenopus*, the EGL is devoid of proliferating cells. (e-g) Quantifications of (A). The ratio of (e) measured URL length and (f) PHH3+ cells in injected side over control side are represented. Each tadpole is represented by a square. (Ac, d) PHH3 positive cells are ectopically detected in the cerebellar plate (Ac, d white arrow heads) of injected embryos. (g) Percentage of PHH3+ cells located inside the URL compared to those located outside the URL were quantified on the injected side and on the control side. (E) The Barhl1-KD induced increase in URL length is rescued upon co-inhibiting Tcf activity. ISH analysis of *n-myc* expression in the cerebellar anlage of stage 48 *X. laevis* embryos unilaterally injected with (Ba) *MObarhl1-1* (15ng), (Bb) *tcf7l1-Δβcat-GR* at 100pg and (Bc) *tcf7l1-Δβcat-GR* at 200pg. *n-myc* marks the boundaries between different rhombomeres which allows the exact measurement of URL length. URL length was rescued when *MObarhl1-1* (15ng) was co-injected with *tcf7l1-Δβcat-GR* at 100pg (Bd) or at 200pg (Be). Ratio of URL length in injected side over control side is represented (Bf). Data are presented as means ± SEM. Each tadpole is represented by a square. Dotted lines separate injected and control sides. Scale bar 150µm. *inj*: injected side; cp: choroid plexus; URL: Upper Rhombic Lip; VZ: Ventricular Zone; R1-R2: Rhombomere 1 and 2; MHB: Midbrain-Hindbrain Boundary. Statistical analysis Ae, Af: was carried out using student's t-test two-tailed. Bf: One-way ANOVA($F_{(4,49)}$=65.1; $p < 0.001$) followed by post hoc Tukey test. ** $p \leq 0.01$; *** $p \leq 0.001$; **** $p \leq 0.0001$.

Figure 6: RNA-sequencing data processing and analysis
(A) Differentially expressed genes (DEGs) visualization Heatmap displaying expression profiles of most significantly upregulated and downregulated DEGs for each condition (*MObarhl1-1 vs MOct* and *MObarhl1-2 vs MOct*). Each row represents a gene, and each column represents a sample. Results are shown as a gradient from blue (downregulated) to dark orange (upregulated). Heatmap is generated using R package. **(B) Volcano plots** showing a selection of significant DEGs with pAdj < 0.001 in (a) *MObarhl1-1 vs MOct* and (b) *MObarhl1-2 vs MOct*. Upregulated genes with Log2FC>0.4, and downregulated genes with Log2FC<-0.4 are shown. Red and blue dots indicate significant DEGs that are upregulated and downregulated, respectively. Grey dots denote RNAs with non-significant difference. PCA and volcano plots were generated using Galaxy. **(C, D) Gene ontology enrichment comparison.** Shown on Y axis are (C) the altered molecular functions and (D) biological processes for selected (C) upregulated (Log2FC≥0.5, PAdj<0.001), and (D) downregulated (Log2FC≤-0.5, PAdj<0.001) DEGs respectively. Enrichment analysis comparing functional profiles among *MObarhl1-1* and *MObarhl1-2* was performed on the DEGs in common between both conditions. Results are visualized as a dot plot based on indicated gene counts and adjusted p-values for enrichment. Dot size corresponds to the count of differentially expressed genes associated with the molecular function or the biological pathway, and dot color refers to the adjusted P-value for enrichment. **(E) Barhl1 and (F) TCF Cis Regulatory Motifs (CRM) in regulatory regions of MOBarhl1 DEGs**: pie chart of % of *MObarhl1* DEGs

located 5Kb or 30Kb upstream or downstream of their TSS as indicated**. (G) ISH analysis of 3 DEGs**: Dorsal views R1 territory of st. 42 *X. laevis* embryos unilaterally injected with *MObarhl1-1* using *hes5.1* as ISH probe *(a) hes5.1, (b) hes5.1 with DMSO, (c) hes5.1 with LY411575*, (d) quantification, (e) Total and average size of the *hes5.1* expression area in embryos grown in LY411757 relative to embryos grown in DMSO. Each tadpole is represented by a square. *inj:* injected side. Statistical analysis was carried out using student's t-test two-tailed. ** $p \leq 0.01$; *** $p \leq 0.001$; **** $p \leq 0.0001$.

A

a

st. 45

n-myc

Forebrain

Midbrain

Rhombomere 1

Hindbrain

Dissected neural tube

b

CP

MHB

n-myc

VZ

R1-R2 boundary

URL

c

Rostral

Lateral

Median

Caudal

VZ

URL

EGL

CP

IGL

B

atoh1

a st.41 | a' st.41 | b st.48 | b' st.48

C

n-myc

a st.41 | a' st.41 | b st.47 | b' st.47

D

hes5.1

a st.42 | a' st.42

hes4

b st.48 | b' st.48

E

pax6

a st.41-42 | a' st.41-42 | b st.47 | b' st.47

F

barhl1

a st.40-41 | a' st.40-41 | b st.48 | b' st.48

G

neurod1

a st.40-41 | a' st.40-41 | b st.48 | b' st.48

H

otx2

a st.40-41 | a' st.40-41 | b st.48 | b' st.48

A

tcf7l1-Δβcat-GR (200pg)

a

atoh1

inj

a'

inj

a''

inj

tcf7l1-Δβcat-GR (100pg)

b

atoh1

inj

b'

inj

b''

inj

tcf7l1-Δβcat-GR

c

- *dex*

+ *dex*

Ratio of atoh1 expression injected side over ct side (Mean of IntDen ± s.e.m)

1.5

1.0

0.5

0.0

***

***

100pg 100pg 200pg

B

tcf7l1-Δβcat-GR (100pg)

a

barhl1

inj

b

pax6

inj

c

neurod1

inj

C

barhl1-GR

a

atoh1

inj

b

pax6

inj

c

neurod1

inj

a'

atoh1

a''

atoh1

inj

B d *tcf7l1-Δβcat-GR (100pg)*

Ratio of expression injected side over ct side (Mean of IntDen ± s.e.m)

4

3

2

1

0

***

***

***

barhl1 *pax6* *neurod1*

C d *barhl1-GR*

- *dex*

+ *dex*

Ratio of expression injected side over ct side (Mean of IntDen ± s.e.m)

4

3

2

1

0

***

**

***

atoh1 *pax6* *neurod1*

Figure 2

A

MObarhl1-1

a

atoh1

inj

a'

a''

inj

b

pax6

inj

B

MObarhl1-2

a

atoh1

inj

a'

a''

inj

b

pax6

inj

C

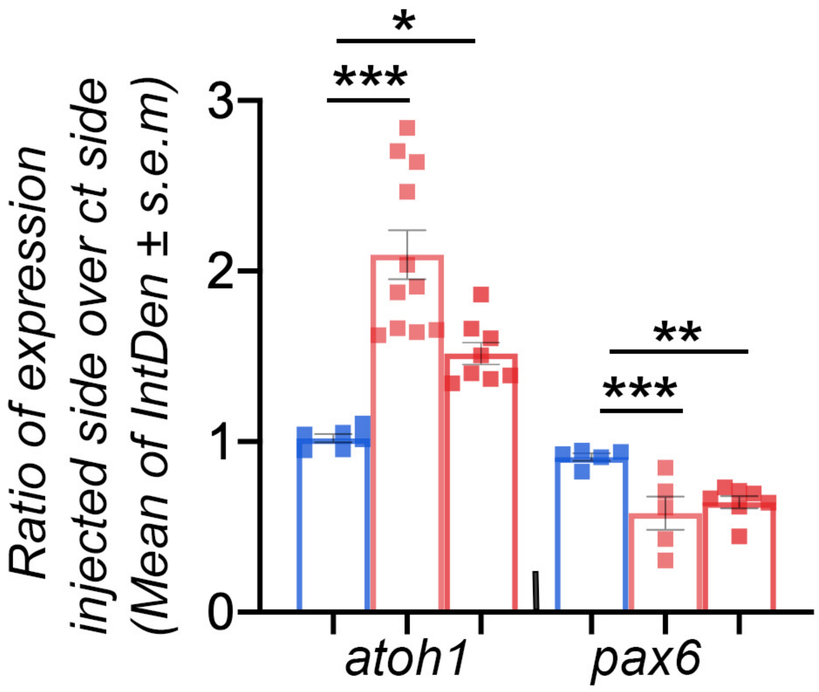

D d

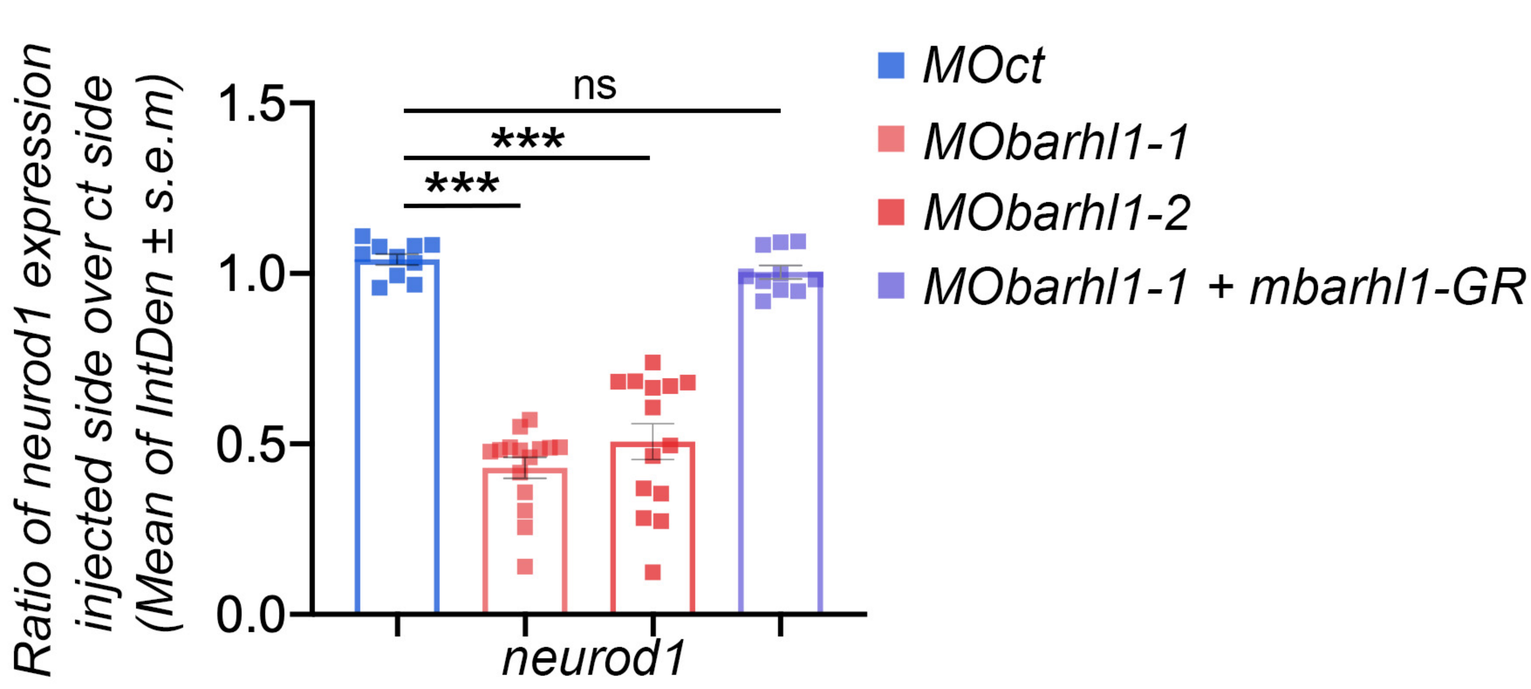

D

MObarhl1-1

a

neurod1

inj

MObarhl1-2

b

neurod1

inj

MObarhl1-1 + mbarhl1-GR

c

neurod1

inj

E

MObarhl1-1

a

pax6

inj

tcf7l1-Δβcat-GR (100pg)

b

pax6

inj

tcf7l1-Δβcat-GR (200pg)

c

pax6

inj

MObarhl1-1 +
tcf7l1-Δβcat-GR (100pg)

d

pax6

inj

MObarhl1-1 +
tcf7l1-Δβcat-GR (200pg)

e

pax6

inj

f

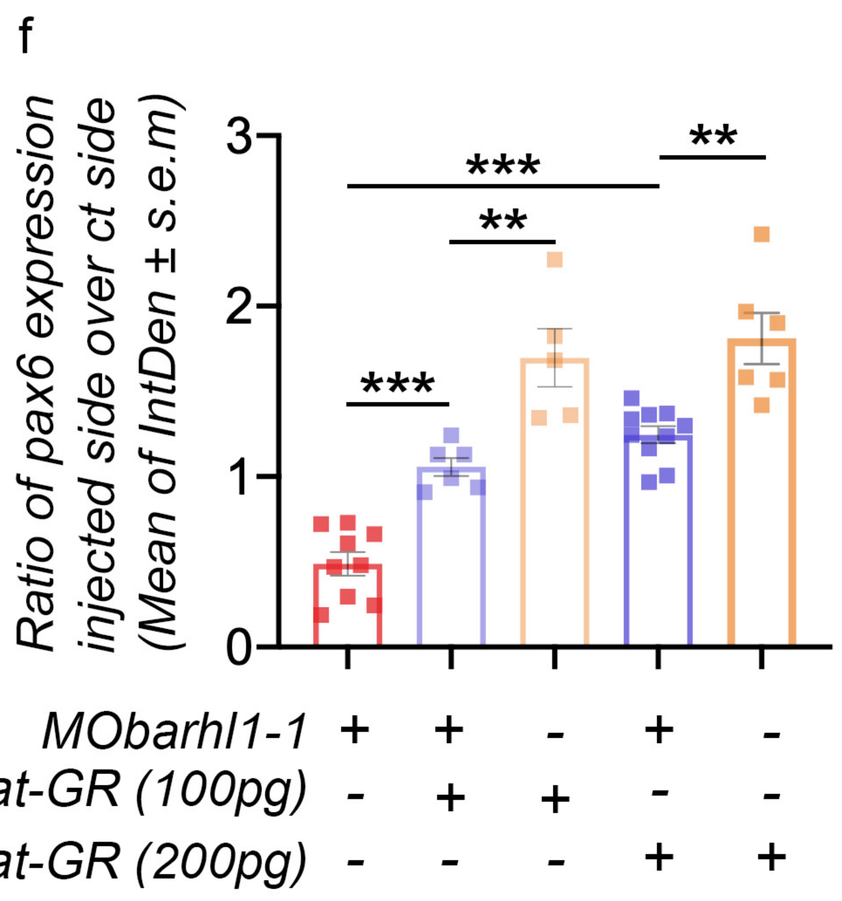

Figure 3

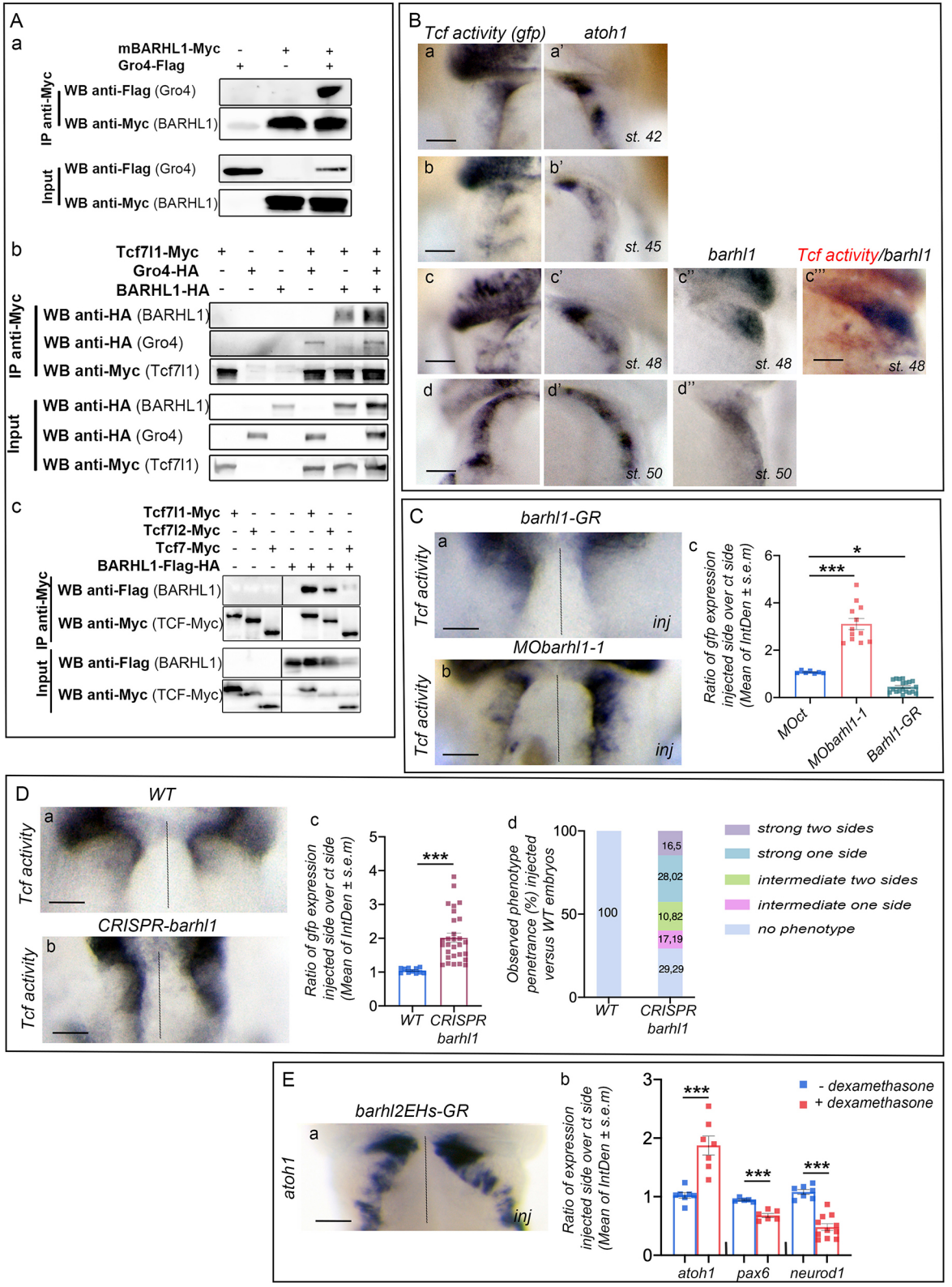
A
a
mBARHL1-Myc
Gro4-Flag
IP anti-Myc
WB anti-Flag (Gro4)
WB anti-Myc (BARHL1)
Input
WB anti-Flag (Gro4)
WB anti-Myc (BARHL1)
b
Tcf7l1-Myc
Gro4-HA
BARHL1-HA
IP anti-Myc
WB anti-HA (BARHL1)
WB anti-HA (Gro4)
WB anti-Myc (Tcf7l1)
Input
WB anti-HA (BARHL1)
WB anti-HA (Gro4)
WB anti-Myc (Tcf7l1)
c
Tcf7l1-Myc
Tcf7l2-Myc
Tcf7-Myc
BARHL1-Flag-HA
IP anti-Myc
WB anti-Flag (BARHL1)
WB anti-Myc (TCF-Myc)
Input
WB anti-Flag (BARHL1)
WB anti-Myc (TCF-Myc)
B
Tcf activity (gfp)
atoh1
barhl1
Tcf activity/barhl1
st. 42
st. 45
st. 48
st. 48
st. 48
st. 50
st. 50
C
barhl1-GR
Tcf activity
inj
MObarhl1-1
Tcf activity
inj
Ratio of gfp expression injected side over ct side (Mean of IntDen ± s.e.m)
MOct
MObarhl1-1
Barhl1-GR
D
WT
Tcf activity
CRISPR-barhl1
Tcf activity
Ratio of gfp expression injected side over ct side (Mean of IntDen ± s.e.m)
WT
CRISPR barhl1
Observed phenotype penetrance (%) injected versus WT embryos
100
16,5
28,02
10,82
17,19
29,29
WT
CRISPR barhl1
strong two sides
strong one side
intermediate two sides
intermediate one side
no phenotype
E
barhl2EHs-GR
atoh1
inj
Ratio of expression injected side over ct side (Mean of IntDen ± s.e.m)
- dexamethasone
+ dexamethasone
atoh1
pax6
neurod1

A

MOct

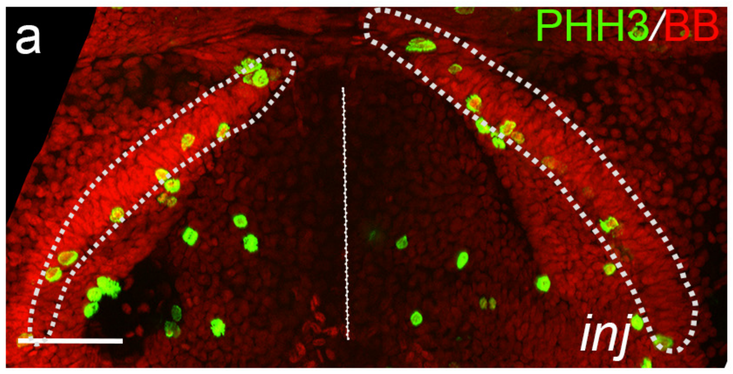

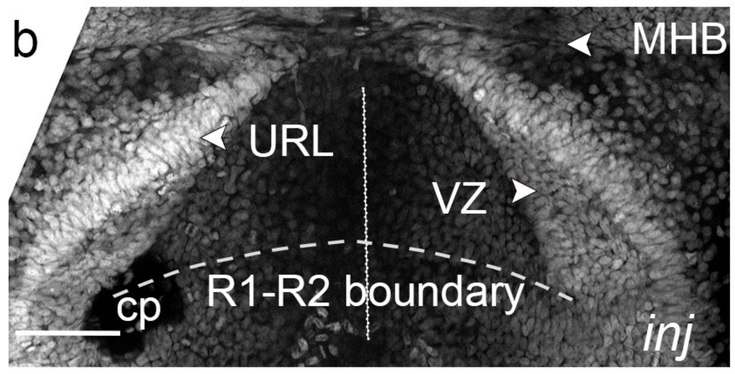

MObarhl1-1

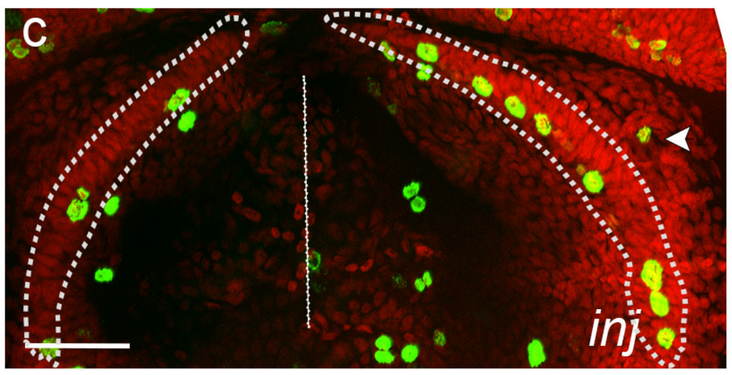

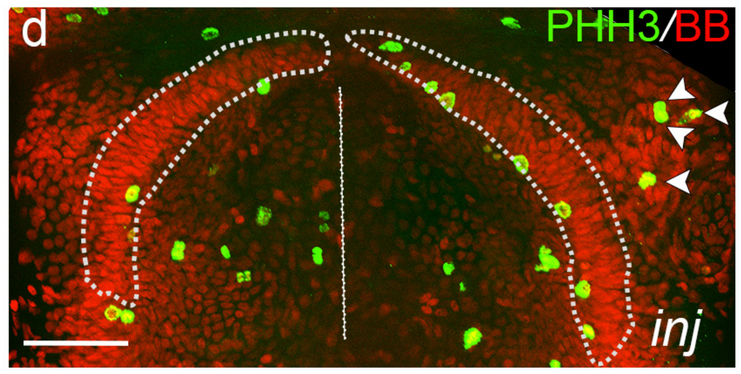

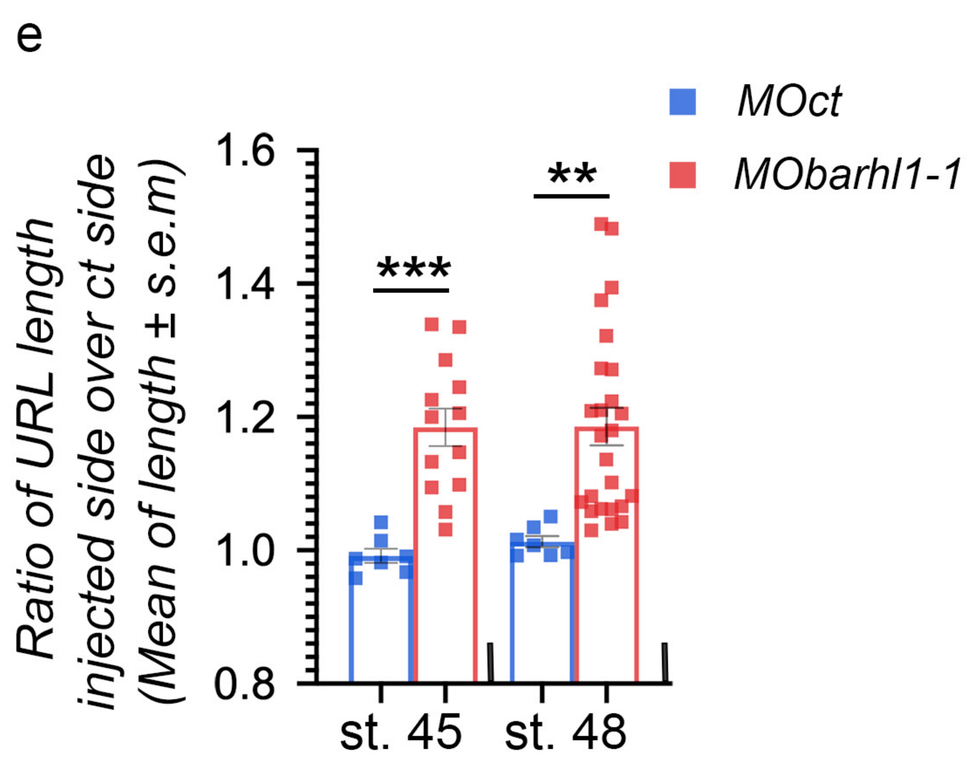

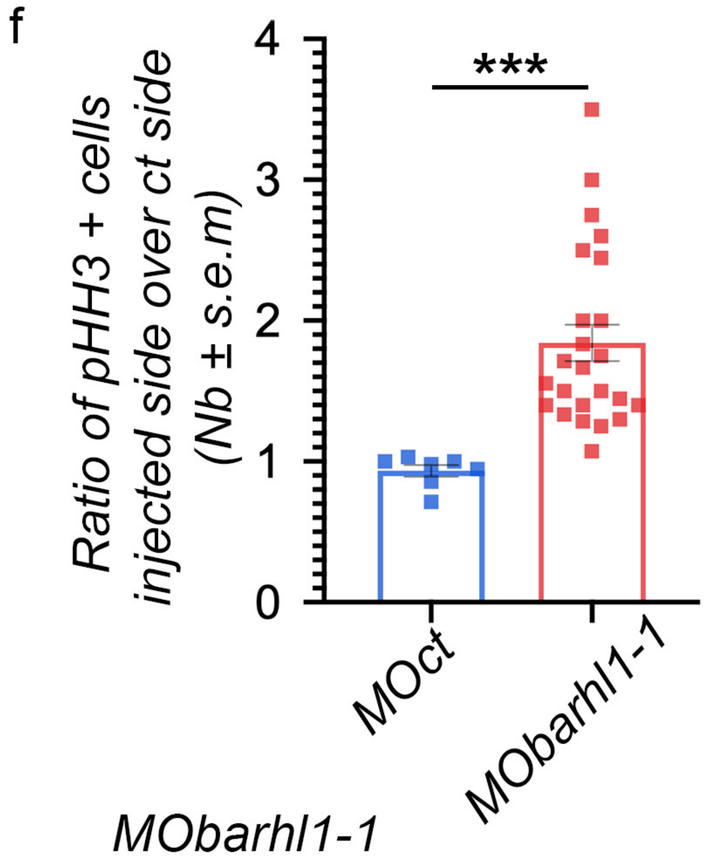

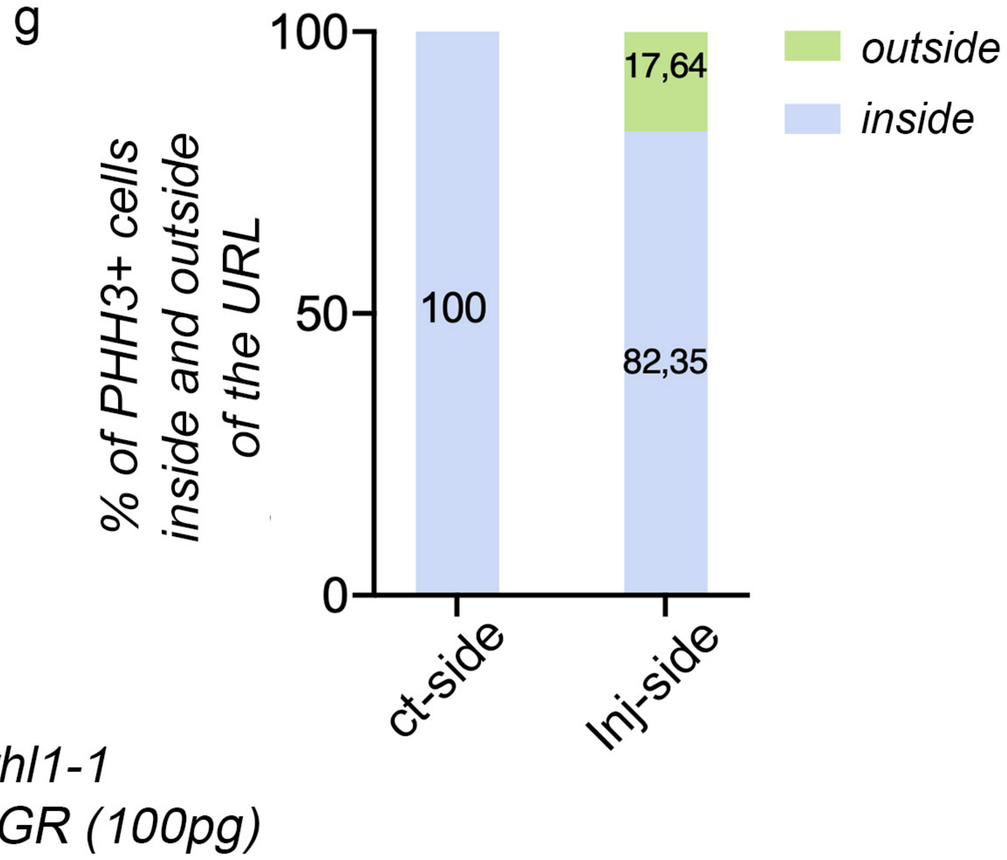

B

MObarhl1-1

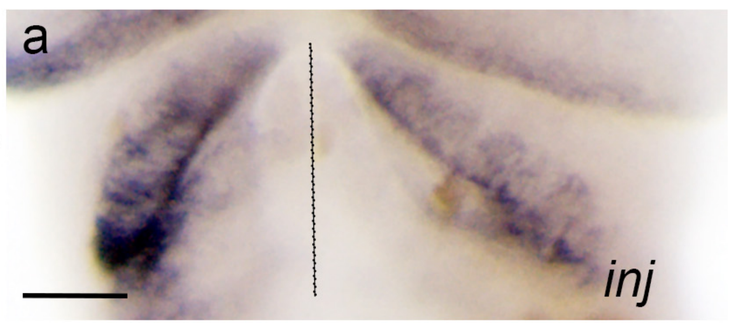

tcf7l1-Δβcat-GR (100pg)

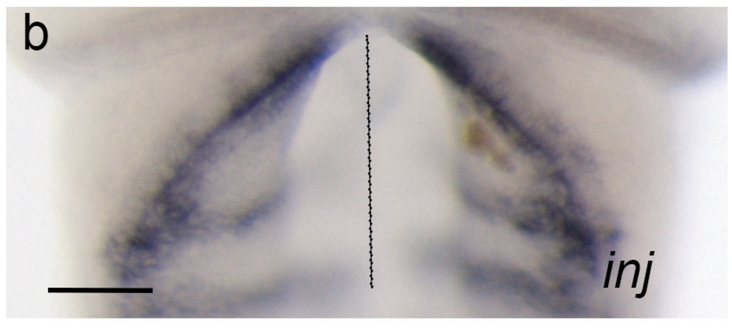

tcf7l1-Δβcat-GR (200pg)

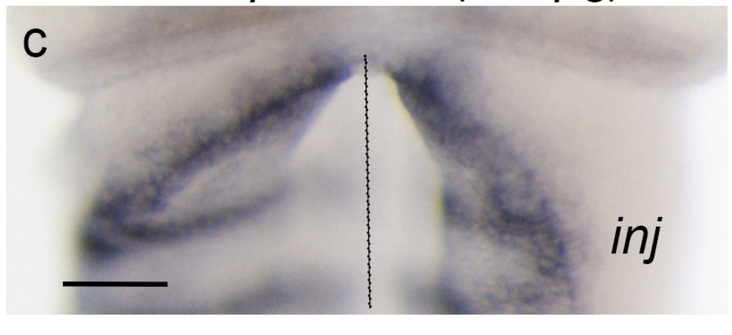

MObarhl1-1
tcf7l1-Δβcat-GR (100pg)

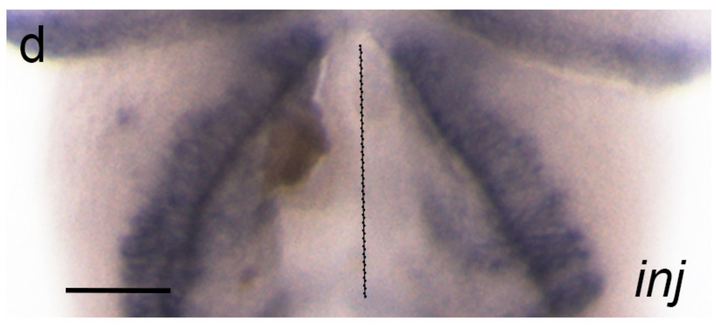

MObarhl1-1
tcf7l1-Δβcat-GR (200pg)

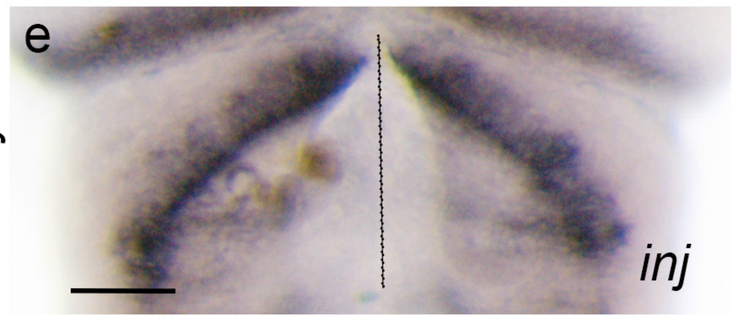

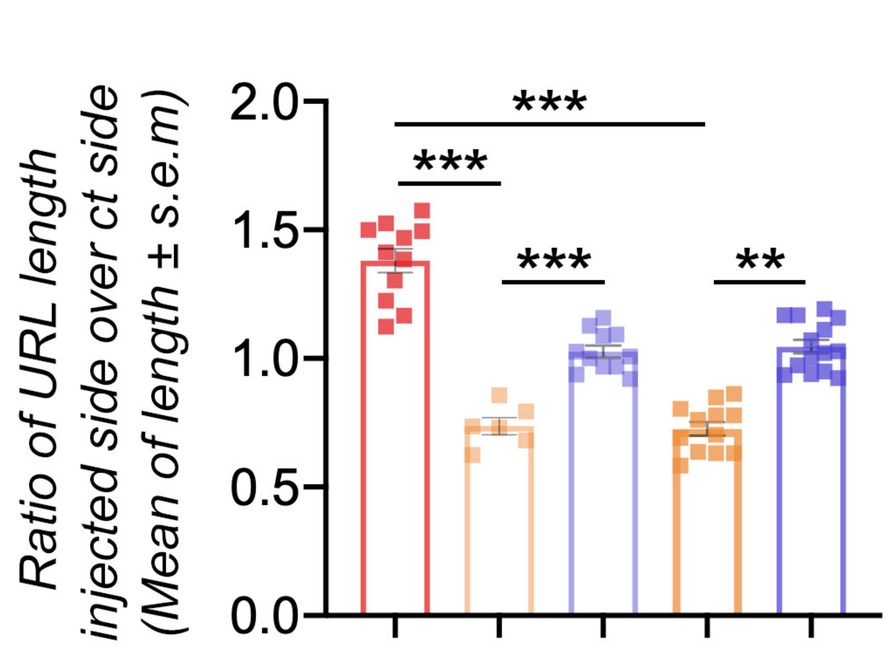

Figure 5

A

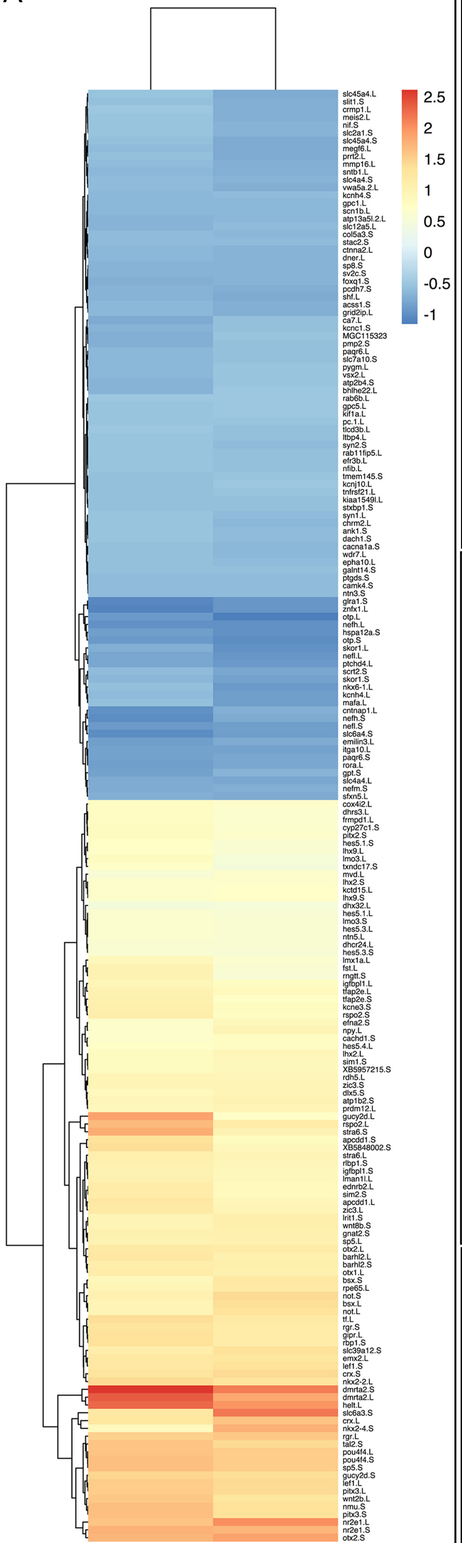

B

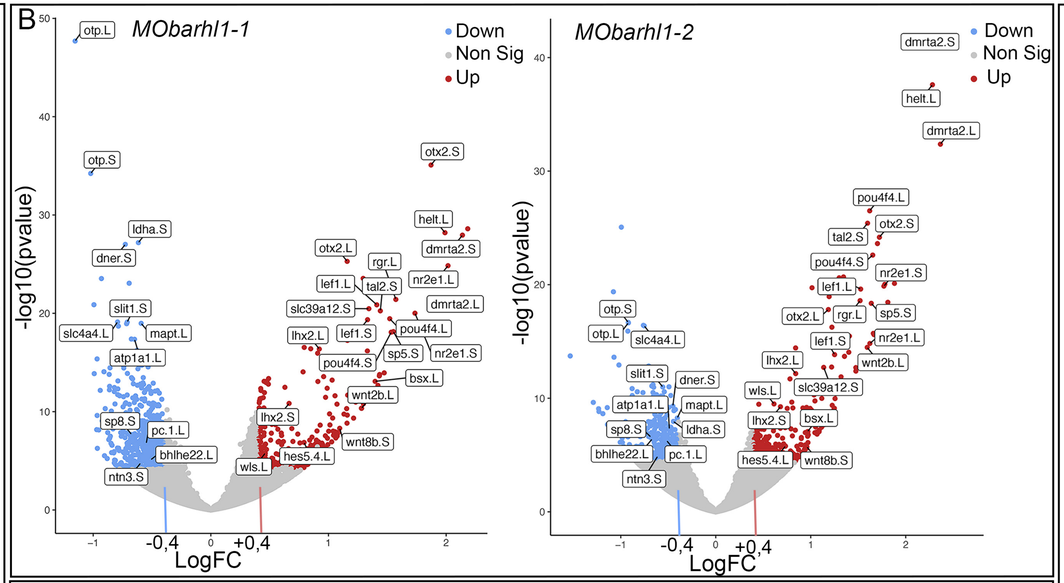

C **Molecular Functions**

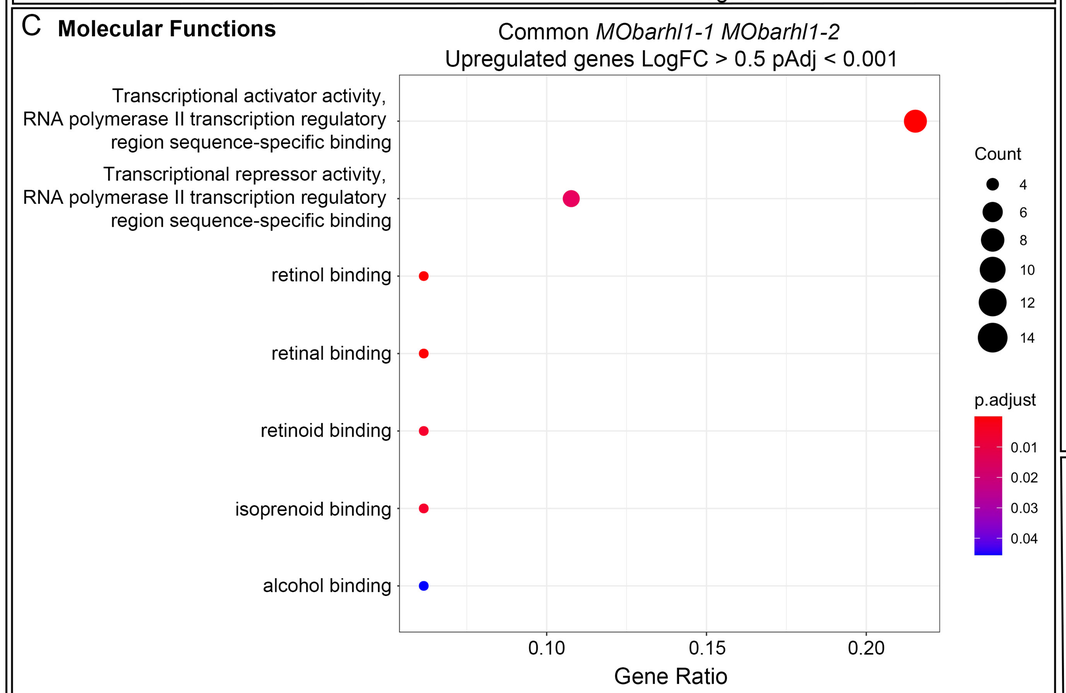

D **Biological Process**

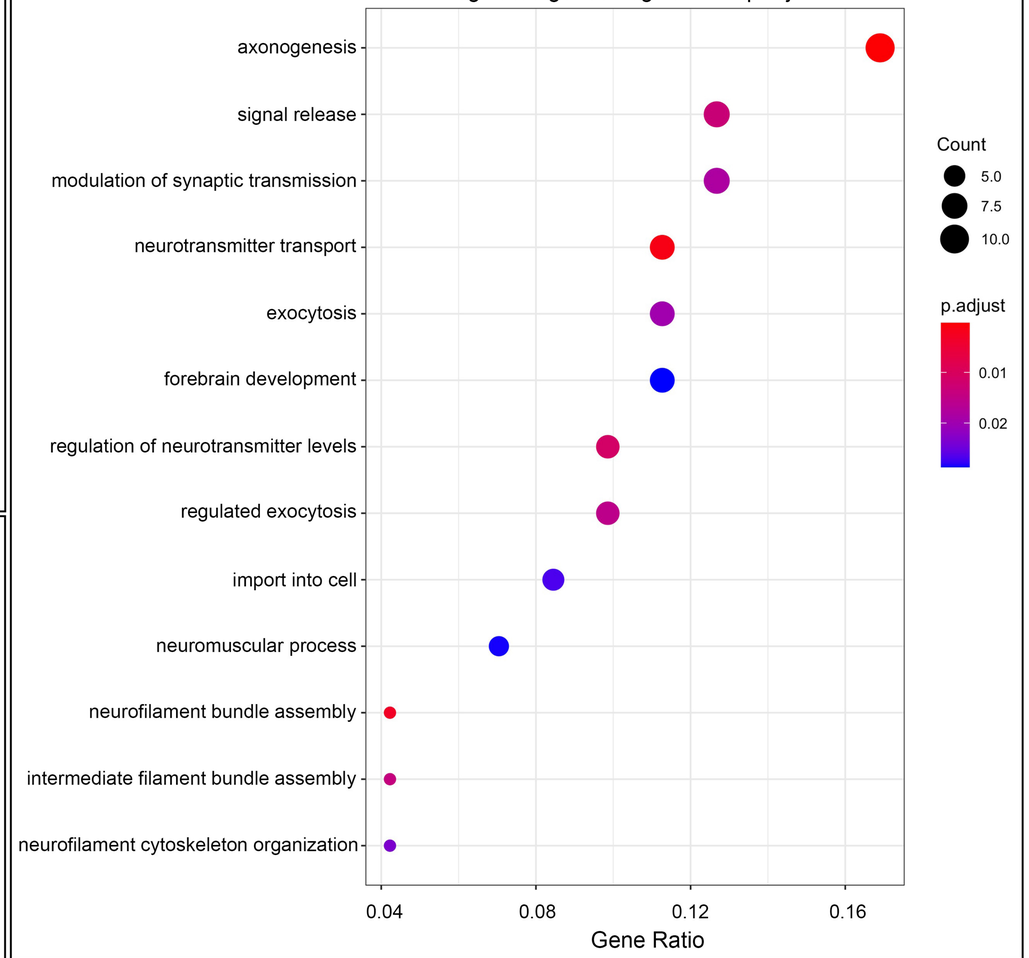

E Barhl1-CRM (5Kb)

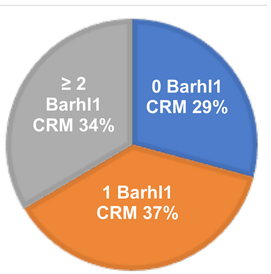

Barhl1-CRM (30Kb)

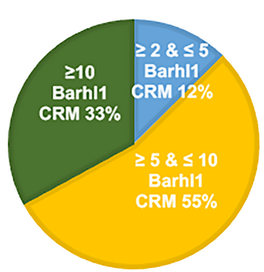

F Tcf-CRM

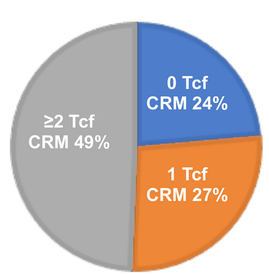

G

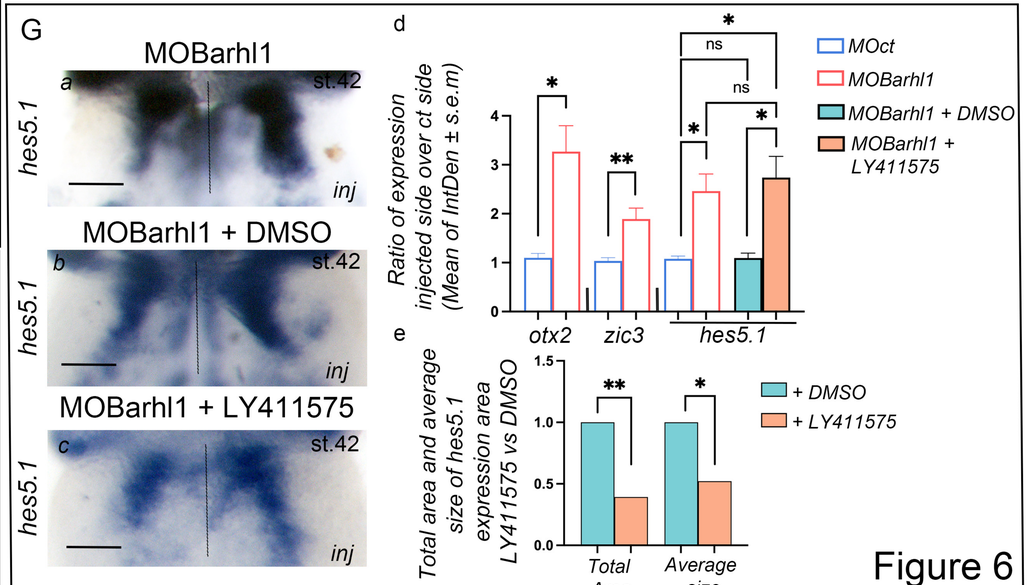

Figure 6

SUPPLEMENTARY FIGURES

Figure S1. Granule neuron progenitors' development in *X. laevis*

Spatial and temporal expression of key markers of GNPs development in the cerebellar anlage of *X. laevis* at indicated stages (st.). Shown are (A-Ea) dorsal view of st. 38 and (A-E) dorsal (b) and lateral (b') views of st. 45 *X. laevis* neural tubes stained with indicated markers. (A) *atoh1* expression is detected in the URL (B) the proliferation marker *nmyc* is expressed in the URL, the VZ, and in proliferating progenitors at the boundaries between the rhombomeres (R). (C) *pax6*+ GNPs are first detected around st. 38 in amphibian. (C, D) *pax6* and *barhl1* mark the committed GNPs while (E) *neurod1* is expressed in differentiated GNs. (F) dorsal view of st. 42 R1 URL showing expression of (a) Tcf7l1, (b) Tcf7l2, (c) tcf7, (d) Lef1. (G) Dorsal views of st. 38, 45 and 48 showing absence of *barhl2* expression in the R1 of amphibian. Scale bar 150µm.

Figure S2. Experimental procedure and constructs

(A) Representation of the injection procedure. mRNAs of the different constructs used in this study (B) were co-injected with a tracer - *gfp* mRNA in *X. laevis* and *mcherry* mRNA in *X. tropicalis* - into one dorsal blastomere at the four/eight-cell stage embryo. Unilaterally injected embryos were selected. On the right is the image of a stage 48 *X. laevis* embryo injected with *gfp* as tracer. Injected and wild-type embryos were left to develop at 18°C. For embryos injected with inducible constructs, half of the injected embryos were treated with 10µM dexamethasone at stage 35, while the other half were untreated and used as control. Embryos were fixed at different stages and used for further analysis by ISH. (B) Schematic representation of the different constructs used in this study. Construct organization is indicated in the drawings. Tcf7l1-Δβcat-GR lacks the β-catenin-binding domain (BCBD) at its N-terminal region (yellow). Absence of this domain reinforces its repressive activity. It contains the DNA-binding domain which contains a High-Mobility Group box (HMG-box) (green) and a Nuclear Localization Signal (NLS) (grey). The DNA-binding domain is preceded by a less well-defined binding sequence for the Groucho/Transducin-like enhancer of split (Gro/TLE) (Gro-binding sequence, GBS) (red). The Context-dependent Regulatory Domain (CRD) is encoded by three exons and is flanked by two small motifs LVPQ shown in blue at its N-terminal end, and SxxSS shown in pink at its C terminal end. The long (E) tail of Tcf7l1 (light blue) contains two C-terminal-binding protein (CtBP) motifs (PLDLS) (purple). This construct is inducible and contains at its Carboxyl (C) terminal end a glucocorticoid receptor/ligand binding domain (GR/LBD). xBarhl1 and mBarhl1 are composed of the full length Barhl1 structure including both N-terminal Engrailed Homology motifs (EH1) (grey and orange), the NLS (light green) followed by the homeodomain (HD) (yellow). xBarhl1 is Flag-tagged. mBarhl1 is Myc tagged. mBarhl1-HA-GR is HA tagged and is inducible. Inducible mBarhl2EHs-GR contains the two EH domains and acts as dominant negative. Western blot was carried out on extract from embryos injected with the mBarhl1-HA-GR and mBarhl2EHs-GR constructs and their expression validated. Samples were separated by SDS-page and detected by immunoblotting with anti-Ha, anti-Flag, anti-Myc, or anti-Barhl2. On the right are shown the molecular weights in kDa. n-inj: non-injected.

Figure S3. Morpholino-mediated depletion of xBarhl1 and its impact on GNPs development

(Aa-c) *MObarhl1-1* and *MObarhl1-2* specifically block translation of *xbarhl1* mRNA. (a, b) Morpholino (MO) oligonucleotides were designed to target the translation initiation site of *X.*

laevis and *X. tropicalis (XL/XT) barhl1* mRNA. *MObarhl1-1* and *MObarhl1-2* do not hybridize with mouse *Barhl1* and *X. laevis barhl2* mRNAs. *X. tropicalis* were injected with *MObarhl1-1.* Red characters indicate nucleotides that do not hybridized with *MObarhl1-1* and *MObarhl1-2*. (c) Western blot on extracts from *X. laevis* embryos injected with flag-tagged *xbarhl1* (*xbarhl1-flag)* together with *MObarhl1-1*, or *MObarhl1-2*, or control MO *(MOct)*. myc-tagged *mBarhl1* (*mBarhl1-myc*) was co-injected with *MObarhl1-1*. *MObarhl1-1* and *MObarhl1-2* induced a dramatic decrease in xBarhl1 protein levels without affecting those of mBarhl1-myc, while *MOct* had no effect on xBarhl1 expression. Membranes were incubated with stripping buffer to eliminate primary anti-flag and secondary antibodies. Asterisk indicates post-stripping xBarhl1-flag corresponding band. Actin was used as loading control to confirm that levels of proteins loaded are equal across the gel. (B) Injection of *MOct* didn't induce any significant effect. *in situ* hybridization analysis of *atoh1, pax6* and *neurod1* expressions in stage 45 *X. laevis* embryos injected with *MOct (20ng).* (C-D) Analysis of *MObarhl1-1* effect at stage 41 and stage 48. ISH analysis of *X. laevis* embryos injected with *MObarhl1-1 (15ng)* report a significant increase in *atoh1* expression and a dramatic decrease in the commitment/differentiation markers *pax6* and *neurod1* at stage 41 and stage 48. Scale bar 150µm.

Figure S4 (A) *in situ* hybridization analysis of *gfp* expression (Tcf activity) performed on *X. tropicalis* pbin7LefdGFP line injected with morpholino control (*MOct).* (B) *in situ* hybridization analysis showing decreased expression of *neurod1* and *pax6* in embryos unilaterally injected with *barhl2EHs-GR. inj:* injected side. Scale bar 150µm. (B) Efficiency of CRISPR/Cas9-mediated mutation of Barhl1 in *X. tropicalis* using T7E1 assay. Representative gel images displaying Polymerase Chain Reaction (PCR) products amplified from genomic DNA isolated from non-injected embryos (ninj) and from embryos injected (inj) with *CRISPRbarhl1-1; CRISPRbarhl1-2; CRISPRbarhl1-3* mixed (a) or each alone (b-c-d) and treated (+T7 digestion) or not (ct: control) with T7E1. PCR product size is 430bp in *ct* samples.

Figure S5. Analysis of count data from RNAseq and Work Flow
(A) **Dispersion plot** showing the dispersion estimates for each gene separately (black points), and the dispersions' dependence on the mean of normalized counts (red line). Final estimates are represented by blue points. The blue circles are genes which have high gene-wise dispersion estimates. (B) **Principal Component Analysis** (PCA) plots were obtained based on RNAseq data aligned with STAR and reads counted using feature-counts. Three samples have been generated for each condition. Sample groups are represented by different colors as indicated. Each dot refers to a sample. Samples showing similar gene expression profiles are clustered together. (C) **Scheme of the RNA-seq work flow** (see Star Methods for details) (D) **Venn-Diagram** showing the distribution of DEGs between *MObarhl1-1 vs MOct* and *MObarhl1-2 vs MOct.* The numbers of DEGs with pAdj<0.001 exclusively expressed by each subset and genes overlapping between both conditions are indicated. Green represents *MObarhl1-1 vs MOct* and light red represents *MObarhl1-2 vs MOct.* Venn diagram is generated using Galaxy. (E) **ISH analysis** of WNT secreted factors or DEGs: Dorsal views R1 territory of st. 42 *X. laevis* embryos either (E) wt, or (F) unilaterally injected with *MObarhl1-1* using as ISH probes (E)*(a) wnt3a, (b) wnt8b, (c) wnt2b and* (F)*(a) otx2, (b) zic3.(G*) **Prevalence of Barhl1 and Tcf CRM** To test the prevalence of CRM for Barhl1 or TCF in non-differentially expressed genes, we randomly selected 232 genes from the list of non-expressed genes and looked for the presence of CRM 5Kb upstream or downstream of DEG TSS. We observed that the number of DEG with regulatory regions (71%) compared to non-DEG with regulatory regions (53%) for Barhl1 is statistically different (chi2 test X2= 7.4355, df = 1, p-value = 0.006). For

TCF, 76% of DEGs had regulatory regions compared to 55% of non-DEGs (chi2 test X2= 19.618, df = 1, p-value < 0.0001).

Table S1: Barhl1 and TCF Cis Regulatory Motif (CRM) on regulatory regions of Barhl1 depleted DEGs. We explore the putative transcription factor-target relationships of Barhl1 (**A**) and Tcf (**B**) on Barhl1 depleted DEGs (PAdj<0.001, Log2FC≥0.45 or Log2FC≤-0.45). We applied R packages Biostrings (v2.64) and GenomicFeatures (v1.48) and determine potential (**A**) Barhl1 binding sites (5'-C-A-A-T-T-A-C/G-3') (and the mirror sequence (5'-G/C-T-A-A-T-T-G-3')) [55], or (**B**) TCF binding sites (5'-C-T-T-T-G-A/T-A-3') (and the mirror sequence (5'-T-A/T-C-A-A-A-G-3')) [56,57] 5Kb upstream and downstream of the Transcription Start Site (TSS) of DEGs using *X. laevis* v10.1 genome assembly downloaded with its corresponding annotation file from Xenbase. For each gene identified through its EntrezID and its symbol, is indicated the sequence of the detected putative CRM and its position within the gene locus.

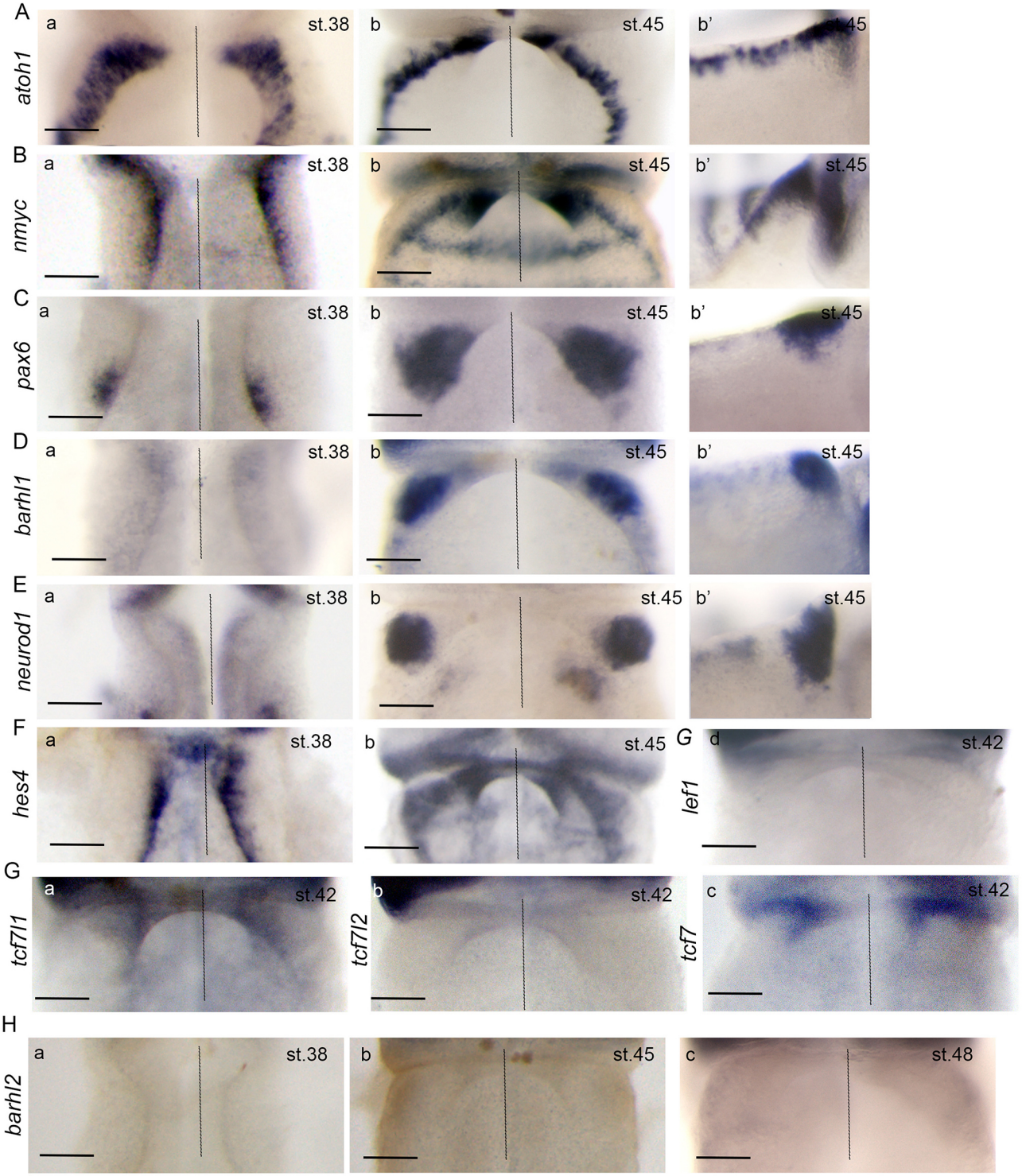

Supplementary Figure 1

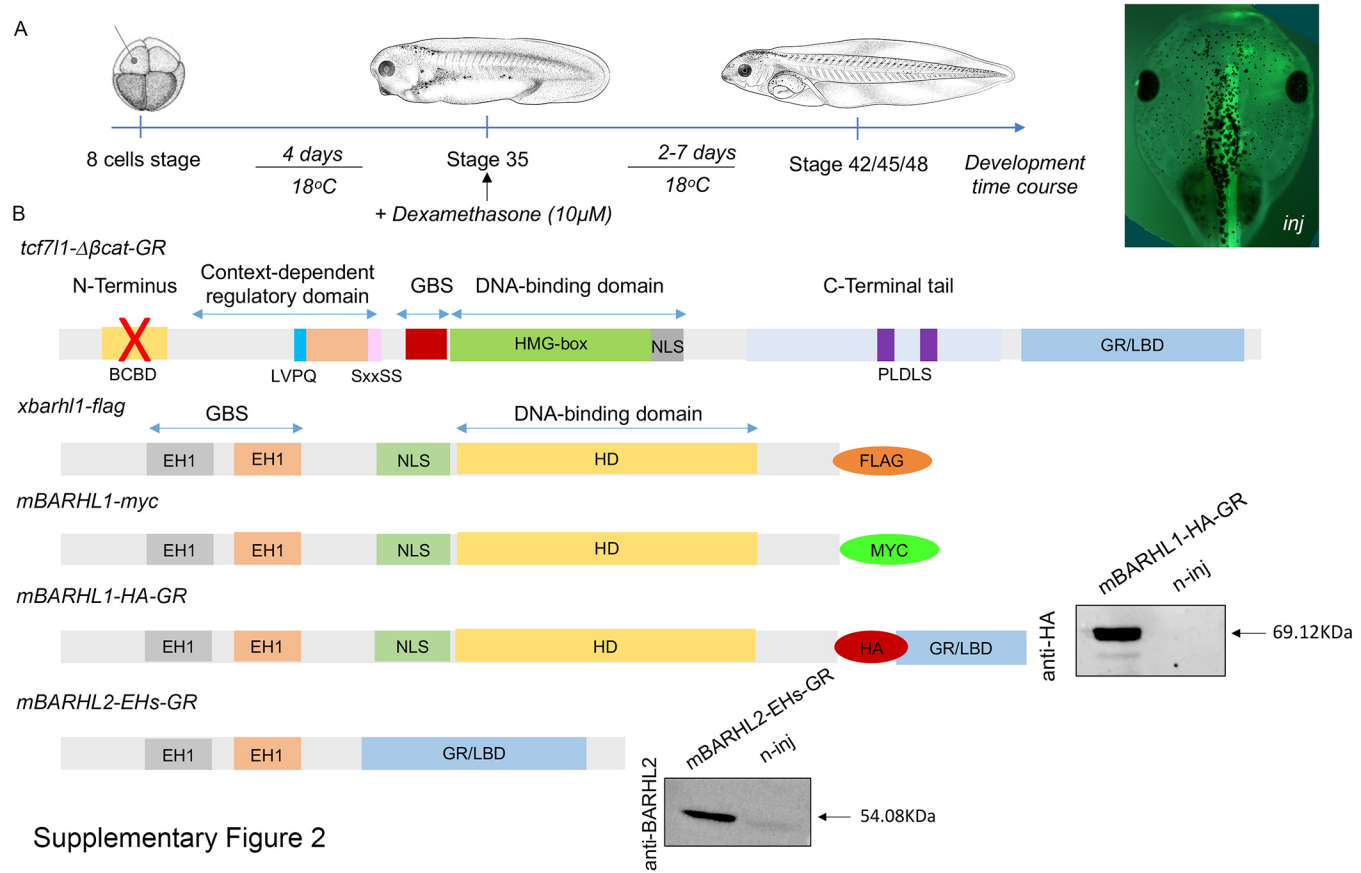

Supplementary Figure 2

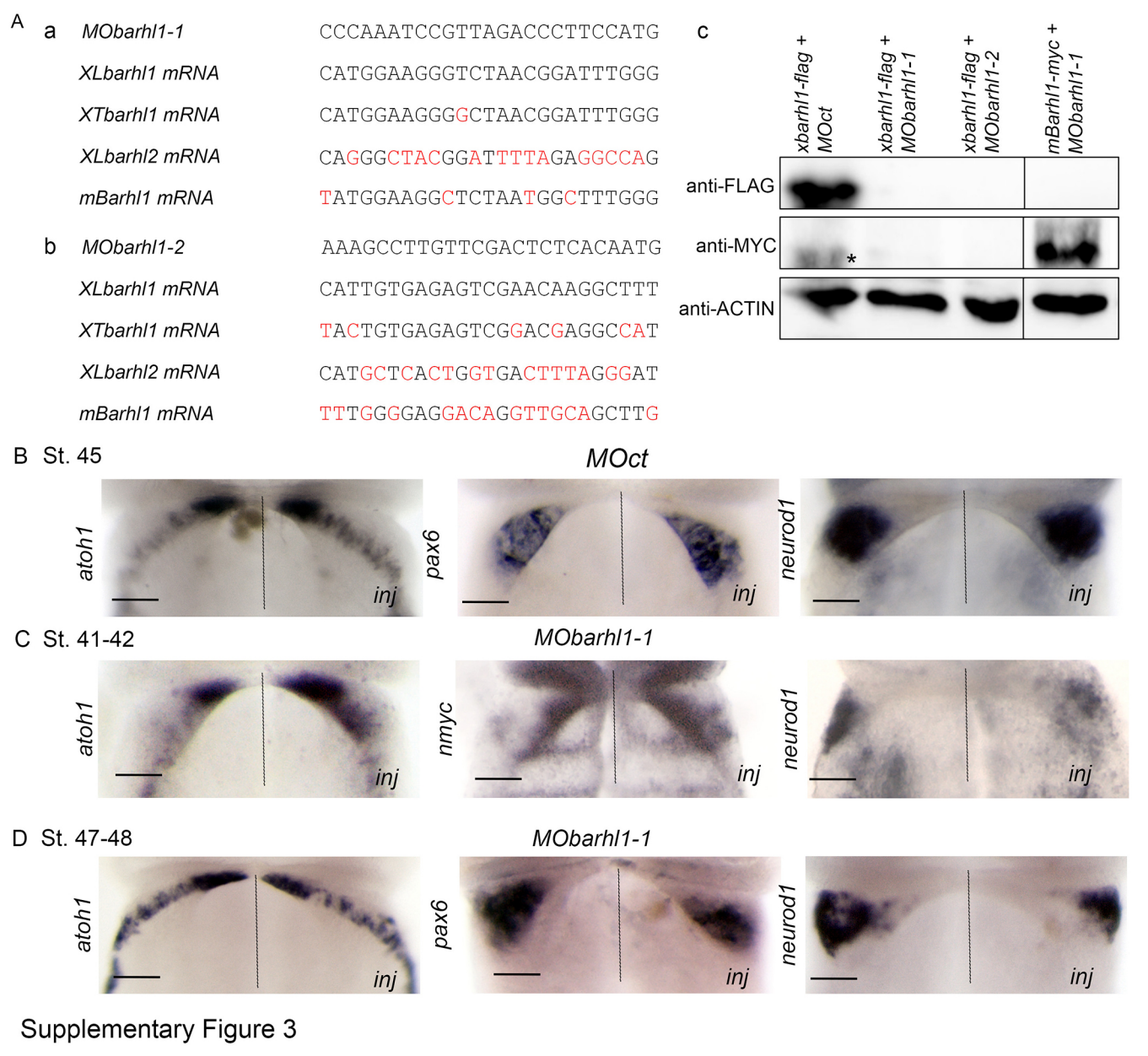

Supplementary Figure 3

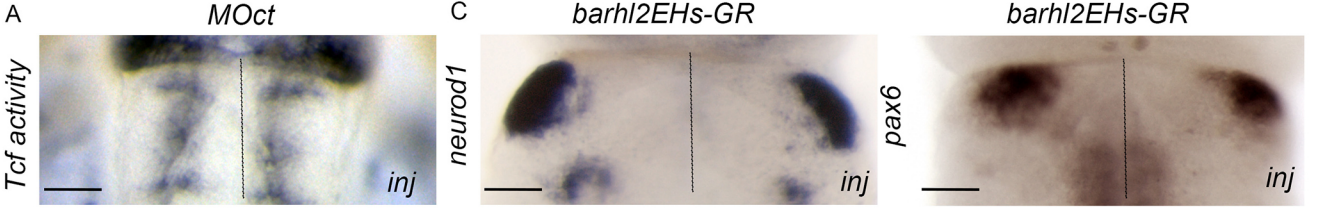

Supplementary Figure 4

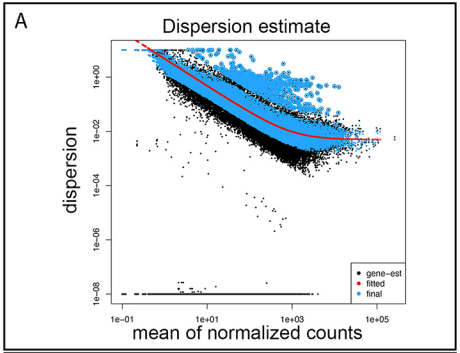

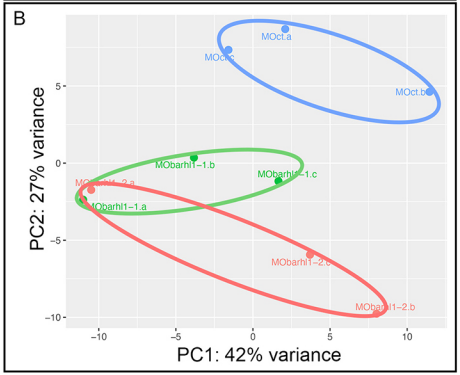

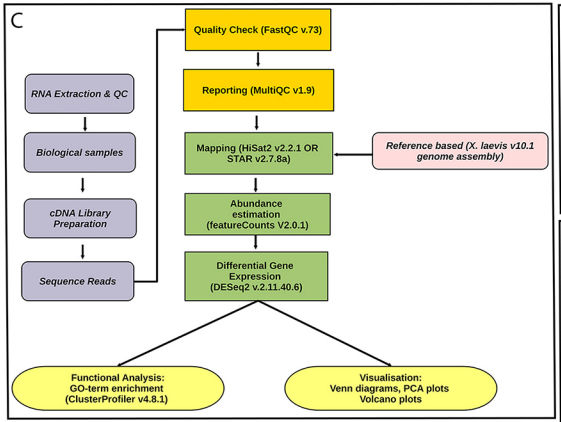

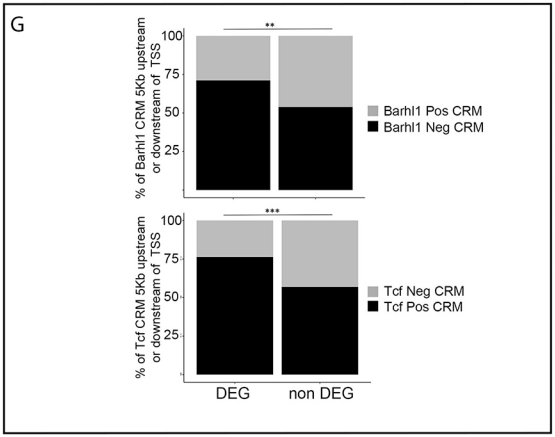

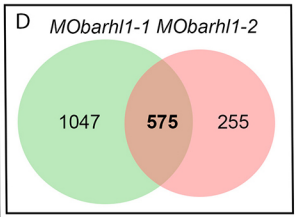

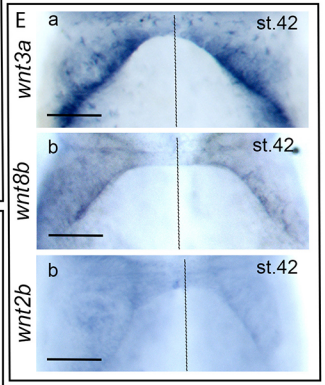

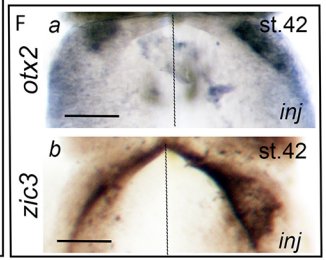

Supplementary Figure 5